
Optimising the KISS readout concept for calorimeter type detectors

Optimierung des KISS Auslese-Konzepts für Kalorimeter-Detektoren

Bachelor-Thesis von Adrian Rost

September 2013



TECHNISCHE
UNIVERSITÄT
DARMSTADT



Optimising the KISS readout concept for calorimeter type detectors
Optimierung des KISS Auslese-Konzepts für Kalorimeter-Detektoren

Vorgelegte Bachelor-Thesis von Adrian Rost

1. Gutachten: Jun.-Prof. Dr. Tetyana Galatyuk
2. Gutachten: Dr. Wolfgang Koenig

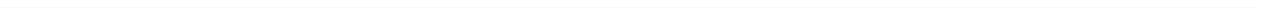
Tag der Einreichung:

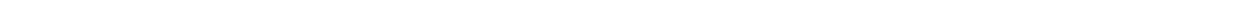
Erklärung zur Bachelor-Thesis

Hiermit versichere ich, die vorliegende Bachelor-Thesis ohne Hilfe Dritter nur mit den angegebenen Quellen und Hilfsmitteln angefertigt zu haben. Alle Stellen, die aus Quellen entnommen wurden, sind als solche kenntlich gemacht. Diese Arbeit hat in gleicher oder ähnlicher Form noch keiner Prüfungsbehörde vorgelegen.

Darmstadt, den 27. September 2013

(Adrian Rost)





Abstract

With the realisation of the FAIR (Facility for Antiproton and Ion Research) accelerator complex in Darmstadt, a new possibility will open to study the microscopic properties of dense baryonic matter at beam energies up to 45 GeV/u. In future two detectors will be able to measure di-leptons in an energy range of the collision system where no data exists. The already running HADES (High Acceptance Di Electron Spectrometer) experiment at GSI Helmholtzzentrum für Schwerionenforschung in Darmstadt, together with the CBM (Compressed Baryonic Matter) experiment, exploring higher beam energies for heavy systems (i.e. Au+Au), will provide new results. Both experiments will use calorimeter type detectors which are read out by photomultiplier tubes (PMTs) or Multi-pixel Avalanche Photo Diodes (MAPDs), respectively. For the read out and digitisation of this detector type a new FPGA (Field Programmable Gate Arrays) based read out electronics and signal digitisation is currently under development. A Charge-to-Digital Converter (QDC) based on a commercial FPGA in a simple design needs to be realised. For this purpose the charge measurement of the detector signal will be transformed into a time measurement, by discharge of the integrated signal linear in time. The TRBv3 (General Purpose Trigger and Readout Board - version 3) will take over the time measurements and data acquisition.

The aim of this work was to study and analyse the detector signals systematically and to optimize the read out electronics. Single Photomultiplier tubes of 1 and 3 inch sizes, planned to be used for the HADES electromagnetic calorimeter (ECAL), were studied. Performance tests of complete ECAL modules equipped with these PMTs were carried out. In addition it was shown, that an FPGA could be used with sufficient resolution as a discriminator.

Zusammenfassung

Mit der Realisierung der FAIR (Facility for Antiproton and Ion Research) Beschleunigeranlagen in Darmstadt werden in naher Zukunft neue Türen in der Untersuchung der mikroskopischen Eigenschaften dichter barionischer Kernmaterie bei Strahlenergien bis zu 45 GeV/u geöffnet. Dafür stehen in Zukunft zwei Detektoren zur Verfügung, welche Di-Leptonen in einem Energiebereich des Stoß-Systems messen werden, in dem bis heute keine Daten zur Verfügung stehen. Das bereits am GSI Helmholtzzentrum für Schwerionenforschung in Darmstadt in diesem Bereich forschende HADES (High Acceptance Di Electron Spectrometer) Experiment wird zusammen mit dem CBM (Compressed Baryonic Matter) Experiment als Weiterentwicklung für höhere Strahlenergien für schwere Systeme (z.B. Au+Au) neue Ergebnisse in diesem Bereich liefern. In beiden Experimenten werden Kalorimeter-Detektoren eingesetzt welche durch Photomultiplier (PMTs) bzw. Multipixel-Avalanche-Photodioden (MAPDs) ausgelesen werden. Für die Auslese und Digitalisierung dieser Detektoren soll eine neuartige auf FPGA's (Field Programmable Gate Arrays) basierende Ausleseelektronik und Signaldigitalisierung entwickelt werden. Genauer soll eine auf kommerziellen FPGAs und einem simplen Design basierende Ladungsmessung realisiert werden. Dafür soll die Ladungsmessung des Detektorsignales durch eine lineare Entladung des integrierten Signals in eine Zeitmessung umgewandelt werden. Das TRBv3 (General Purpose Trigger and Readout Board - Version 3) wird dabei die Zeitmessung und Datenakquisition übernehmen.

Ziel dieser Arbeit war es die Detektorsignale systematisch zu analysieren und zu verstehen, um die Ausleseelektronik optimal an diese anpassen zu können. Einzelne Photomultiplier mit Größen von 1 und 3 Inch, welche im HADES ECAL Detektor eingesetzt werden sollen, wurden untersucht. Leistungstests von kompletten mit diesen Photomultipliern ausgestatteten ECAL Modulen wurden durchgeführt. Es konnte außerdem gezeigt werden, dass ein FPGA mit hinreichend guter Auflösung als Diskriminator verwendet werden kann.

Contents

1	Introduction	1
1.1	The HADES experiment at GSI Helmholtzzentrum für Schwerionenforschung	1
1.1.1	The electromagnetic calorimeter (ECAL) for HADES	1
1.2	The CBM experiment at FAIR	3
1.2.1	The Projectile Spectator Detector (PSD) of CBM	4
2	Calorimetry detectors for HADES and CBM at FAIR	5
2.1	Physics of calorimeter detectors	5
2.2	General calorimeter read out techniques: PMTs and MAPDs	9
2.2.1	The Photomultiplier Tube (PMT) and common technical problems and challenges	9
2.2.2	The Multi-pixel Avalanche Photo Diode (MAPD)	12
2.3	HADES ECAL module properties	13
2.4	CBM PSD module properties	14
3	The COME and KISS read-out concept	15
3.1	The COME and KISS read-out concept for the ECAL detector in HADES	15
3.1.1	HADES ECAL read-out requirements and general read-out scheme	15
3.1.2	COME and KISS charge-to-width (Q2W) measurement with an FPGA - the PaDiWa AMPS front-end board	17
3.1.3	State-of-the-art simulations of the Q2W-electronics	18
3.2	Possible applications of the COME and KISS readout concept	19
4	First COME and KISS measurements	21
4.1	Installation of a test set-up to characterize calorimeter type detectors and their read-out electronics	21
4.1.1	HADES ECAL test set-up	22
4.1.2	CBM PSD test set-up	23
4.1.3	PaDiWa + TRBv3 test set-up	23
4.2	KISS measurements with a commercial oscilloscope	24
4.2.1	The readout principle and its intrinsic resolution	24
4.2.2	Proof of principle: readout electronics resolution and single photo electron peaks from a MAPD	27

4.3	Characterisation of HADES ECAL PMTs	28
4.3.1	Identification of spurious pulses in 3 inch HAMAMATSU R6091 PMTs	28
4.3.2	Amplitude/gain stability of 3 inch HAMAMATSU R6091 PMTs	31
4.3.3	Uniformity of light collection of 3 inch HAMAMATSU R6091 PMTs	31
4.3.4	(Earth) magnetic field influences on 3 inch HAMAMATSU R6091 PMTs	32
4.4	Determination of a lower boundary of the energy resolution of HADES ECAL modules	35
4.4.1	Photon statistics limitation of ECAL modules resolution equipped with 3 inch HAMAMATSU R6091 PMT	35
4.5	Photon statistical properties of ECAL modules with 1 inch HAMAMATSU R8619 PMTs	37
4.6	Performance tests of HADES ECAL modules with cosmic muons	38
4.6.1	Energy resolution comparison of ECAL modules with 1 and 3 inch PMTs	38
4.7	First steps towards the PaDiWa AMPS Q2W front-end electronic	42
4.7.1	Proof of principle: FPGA used as discriminator	42
4.7.2	Optimal decay slope for the Q2W electronics	42
4.7.3	Impact of the discriminator resolution onto the relative signal-charge resolu- tion	44
<hr/> 5 Summary and outlook		45
<hr/> List of Figures		47
<hr/> Bibliography		49

1 Introduction

With the realisation of the FAIR accelerator complex in Darmstadt, a new possibility will open to study the microscopic properties of dense baryonic matter at beam energies up to 45 GeV/u. In future two detectors will be able to measure di-leptons in an energy range of the collision system where no other data exists. The already running HADES experiment at GSI Helmholtzzentrum für Schwerionenforschung in Darmstadt, together with the CBM experiment, as an extension to higher beam energies, will provide new results. Both experiments will use calorimeter type detectors, which are read out by photomultiplier tubes (PMTs) and Multi-pixel Avalanche Photo Diodes (MAPDs) respectively. A short introduction into the physics of the HADES and CBM experiment and calorimeter type detectors will be given in the following.

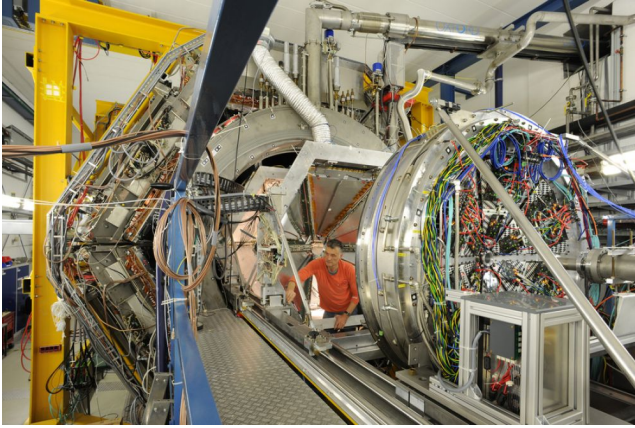
1.1 The HADES experiment at GSI Helmholtzzentrum für Schwerionenforschung

The *High Acceptance DiElectron Spectrometer* (HADES) at GSI Helmholtzzentrum für Schwerionenforschung in Darmstadt allows high resolution measurements of e^+e^- pairs (di-electrons) [5][2][4][6] and charged hadrons, which are produced in elementary and heavy-ion reactions at beam energies of 1 - 3.5 GeV/u at the SIS18 (heavy ion accelerator, 18 Tm rigidity) synchrotron. The main physics aim is to investigate the properties of dense baryonic matter at moderate temperatures. Currently the possibilities of di-electron measurements in heavy ion collisions are up to Au+Au exploited. [3]

The spectrometer covers polar angles from 18° up to 85° and nearly full azimuthal angle of 360° . The track reconstruction efficiency is 90% (for particles with momenta > 500 MeV/c) and a mass resolution in the vector mesons region (800 MeV/c²) of 15 MeV/c² is achieved. The identification of electrons, pions, kaons and protons is possible by combinations of time-of-flight, momentum and energy loss measurements. The main detector components are a START-TARGET-VETO system, a Ring Imaging Cherenkov Detector (RICH), four Multiwire Drift Chambers (MDC), two in front and two behind the Iron Less Superconducting Electro Magnet (ILSE), Resistive Plate Chambers (RPC) based time-of-flight wall, as well as a scintillator based Time of Flight Wall (TOF), a Pre-Shower detector (Pre-SHOWER), a Forward hodoscope Wall (WALL) and a high performance Data Acquisition System (DAQ). A photograph and a schematic view of the HADES spectrometer are shown in Fig. 1.1. The Pre-SHOWER detector will be replaced in future by an electromagnetic calorimeter (ECAL).

1.1.1 The electromagnetic calorimeter (ECAL) for HADES

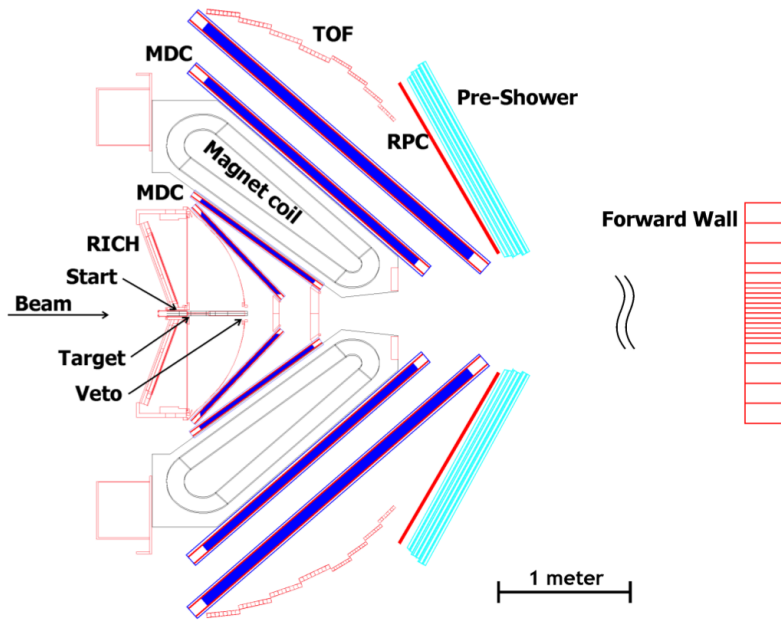
At SIS100 energies, at the planned *Facility for Antiproton and Ion Research* (FAIR), the HADES spectrometer will be placed in front of the *Compressed Baryonic Matter* (CBM) experiment, to continue its physics program at collision energies from 2 to 11 GeV/u. An *electromagnetic calorimeter*



(a) Front-view (in beam direction): The RICH detector (right) as well the innermost MDC plane are in service position.



(b) Back-view: Pre-SHOWER detector (right) and Forward hodoscope Wall (left).



(c) Schematic view of the detector set-up.

Figure 1.1: The HADES experiment at the GSI Helmholtzzentrum für Schwerionenforschung in Darmstadt. The Pre-SHOWER detector will be replaced in future by the ECAL detector [21]. (Pictures by Gabi Otto, GSI)

(ECAL) is foreseen to replace the Pre-SHOWER detector in order to measure π^0 and η meson yields via their two photon decay. Also ω vector mesons could be reconstructed via their decay channel $\omega \rightarrow \pi^0\gamma \rightarrow \gamma\gamma\gamma$, as well as direct photons and photons coming from decays of neutral $\Lambda(1405)$ and $\Sigma(1385)$ resonances and other strangeness containing particles. It will also significantly improve the electron/pion separation at large momenta ($p > 400 \text{ MeV}/c$) (see Fig. 1.2 (left)).

The ECAL detector will be built from 978 lead glass modules, recycled from the OPAL End-Cap calorimeter at CERN [25][15]. The modules will be arranged in six sectors, mounted on a movable support structure. It will cover mostly full azimuthal and polar angles from 12° to 45° . The design energy resolution for photons and electrons is about $6\%/\sqrt{E[\text{GeV}]}$. A 3D model of the HADES ECAL detector is shown in Fig. 1.2 (right).

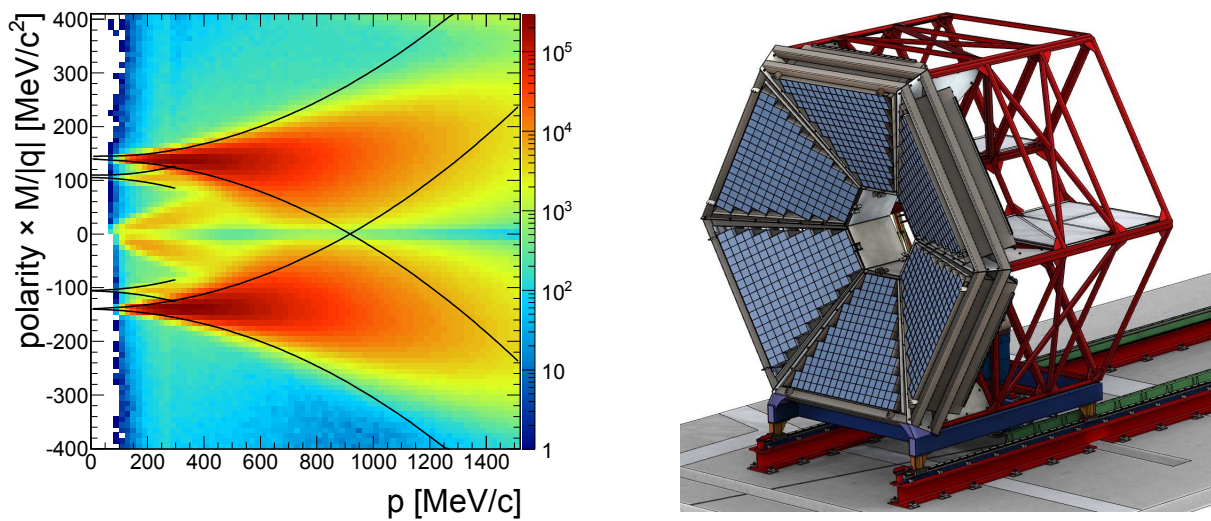


Figure 1.2: Left: $M/|q|$ times polarity as a function of particle momentum p reconstructed with the RPC detector. Electron/pion separation at large momenta can only be improved by including an electromagnetic calorimeter (ECAL) into the HADES set-up [12]. Right: 3D model of the HADES ECAL detector [9].

1.2 The CBM experiment at FAIR

The *Compressed Baryonic Matter* (CBM) experiment [10], at the future *Facility for Antiproton and Ion Research* (FAIR) accelerator complex (SIS100/300), will explore the phase diagram of strongly interacting matter in the region of high baryon densities. The detector will be able to provide data for beam energies up to 45 GeV/u. The physic program will focus on the search of the phase transition between hadronic and quark-gluon matter, the possible existence of a quantum chromodynamics (QCD) critical endpoint, new forms of exotic matter, in-medium modifications of hadrons and the possible relation to chiral symmetry restoration.

The CBM set-up will consist of a large acceptance dipole magnet, a radiation-hard Silicon Pixel Detector System (STS) and a Multi Vertex Detector system (MVD) for tracking and vertex determination, a Ring Imaging Cherenkov Detector (RICH) and Transition Radiation Detectors (TRD) for

electron identification, Resistive Plate Chambers (RPC) for time-of-flight measurement, an Electromagnetic Calorimeter (ECAL) and a Projectile Spectator Detector (PSD) for centrality and reaction plane determination. A 3D model of the CBM set-up (the di-electron option) is shown in Fig. 1.3. As an alternative to the di-electron measurement via a RICH detector, a muon spectrometer consisting of a sandwich of iron shielding and tracking detectors is planned as well.

The PSD detector will be build of 44 lead scintillator sampling calorimeter modules. The detector will be the last detector, located about 16 m behind the target and covering an area of about 2 m² (in the detector set-up for SIS300).

1.2.1 The Projectile Spectator Detector (PSD) of CBM

For studies concerning collective flow, a well-defined reaction plane has to be determined by a method which will not involve the particles, participating in the collision. The *Projectile Spectator Detector* (PSD) [30] is a detector to measure the number of non-interacting nucleons from a projectile nucleus in nucleus-nucleus reactions to determine the collision centrality and the orientation of the reaction plane.

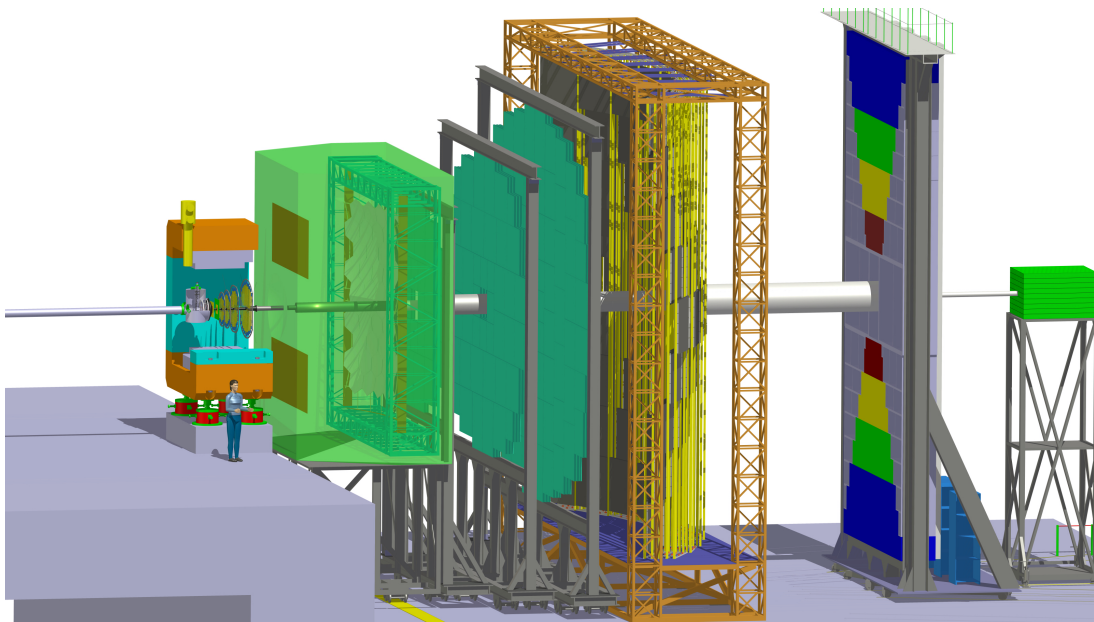


Figure 1.3: The CBM experiment in its electron detection option. The detector consist of (from left to right) a large acceptance dipole magnet, a Silicon Pixel Detector (STS), a Multi Vertex Detector (MVD), a Ring Imaging Cherenkov Detector (RICH), Transition Radiation Detectors (TRD), Resistive Plate Chambers (RPC), an Electromagnetic Calorimeter (ECAL) and a Projectile Spectator Detector (PSD) [30].

2 Calorimetry detectors for HADES and CBM at FAIR

In high energy physics experiments calorimeter detectors are important tools to measure the energy of particles. In this chapter a short introduction into calorimeter detectors and their readout via Photomultiplier tubes (PMTs) and Multi-pixel Avalanche Photo Diodes (MAPDs) will be given. Also the calorimeter module requirements for the HADES ECAL detector and the CBM PSD detector will be briefly discussed.

2.1 Physics of calorimeter detectors

In high energy physics experiments, a calorimeter detector are used to measure directly the kinetic energy of particles. The basic principle is to stop an incoming particle in an absorber material and measure its deposited energy. *Electromagnetic calorimeters* are used to detect particles by their interaction with the material via the electromagnetic force (i.e. electrons, photons) and *hadronic calorimeters* for particles interacting via the strong force (hadrons: i.e. protons, pions, kaons, neutrons). In Fig. 2.1 a typical detector arrangement used in high energy physics experiments and the interaction of different particles is schematically shown. Generally, calorimeters can be divided into two types. On one hand, there are *homogeneous calorimeters* which are made of one layer where the same medium plays a role as energy absorber and detection material. On the other hand, there are *sampling calorimeters*, where absorber and detection media are separated. The detection is based on the measurement of scintillation light (i.e. scintillator crystals, liquid noble gases), ionization (i.e. liquid noble gases) or the measurement of Cherenkov radiation (i.e. lead glass). The produced signal in the detection material is proportional to the deposited energy of the incoming particle. A lead scintillator sandwich calorimeter which is built of sequential layers of lead as absorber and a scintillator as detection material is an example of this type of calorimeter.

In the following, the physics of a homogeneous electromagnetic lead glass calorimeter will be discussed, since this type of detector in the future will be used in HADES. The calorimeter will be built out of boxed elements of lead glass, coupled to a photomultiplier tube, called module. Each module consists of a lead glass block with a length of 420 mm. When, for example, a photon with an energy over 1 MeV enters the lead glass the probability for pair production is large. The produced e^+e^- pair emits again photons via a Bremsstrahlung process. These photons can produce again e^+e^- pairs, hence an electromagnetic shower is developing. Simplified one can assume that the number of shower particles (γ, e^+e^-) in a depth $t = x/X_0$, normalised to the radiation lengths X_0 is:

$$N(t) = 2^t. \tag{2.1}$$

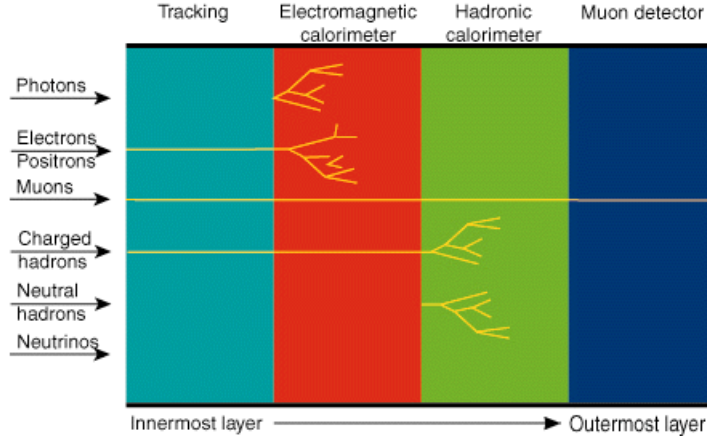


Figure 2.1: Typical arrangement of detectors used in high energy physics experiments and the interaction of different particles [1].

In Fig. 2.2 an idealized electromagnetic shower development is shown. The mean energy of each particle at depth t , can be calculated by

$$E(t) = E_0 \cdot 2^{-t}. \quad (2.2)$$

This process continues until the particle energy falls below the critical energy $E_0/N = E_C$, where Compton scattering and photoelectric effect for photons and ionization for electrons become dominant. The shower maximum and its end is reached when $E_C = E_0 \cdot 2^{-t_{max}}$ is fulfilled, from which follows:

$$t_{max} = \frac{\ln(E_0/E_C)}{\ln(2)}. \quad (2.3)$$

Fig. 2.3 shows a Monte Carlo simulation of a lead glass module of the HADES ECAL detector with a radiation length of $X_0 = 2.51$ cm, performed with HGeant2 (a HADES simulation package, based on the CERN software GEANT 3.21). The shower development for electrons, photons, muons and protons with different energies hitting the lead glass perpendicular from the left are shown. The shower generated by electrons and by photons are similar. By going up in energy the shower goes deeper into the module (see equation 2.3) and the development of secondary particles increases. Since HADES ECAL lead glass modules are electromagnetic calorimeters, particles like muons and protons show less interaction with the material and only a fraction of their kinetic energy deposited.

In lead glass calorimeters the Cherenkov effect is used to determine the deposited energy. Charged particles, which are created in the shower process, may travel through the lead glass at a speed greater than the velocity of light in that medium. Hence Cherenkov radiation is emitted by those particles in a Mach cone, which can be described by,

$$\cos(\theta) = \frac{1}{n\beta}. \quad (2.4)$$

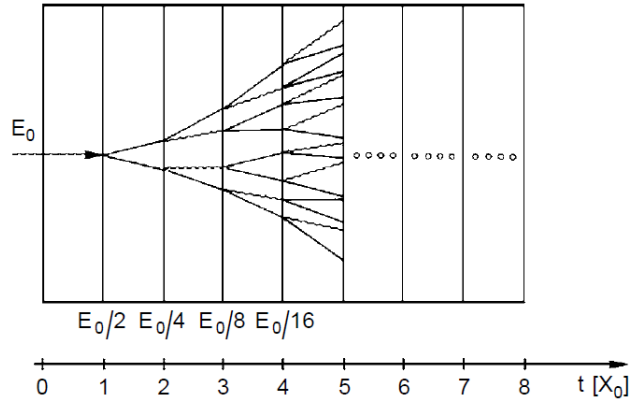


Figure 2.2: Idealized electromagnetic shower production in a calorimeter. The wavy lines are photons and the continuous lines are electron tracks. The material length t is given in radiation length units X_0 [14].

where n is the refraction index of the medium and θ the half of the opening angle of the Mach cone. For example, a cosmic muon (velocity $\beta \approx 1$) travelling through a lead glass module with an refraction index $n = 1.708$, it will emit Cherenkov light in a Mach cone with $\theta = 54^\circ$.

The Cherenkov radiation threshold energy for electrons in lead glass is quite low $T_C^E \approx 120$ keV, implying that the total number of Cherenkov photons is approximately proportional to the total track length of all charged particles which are produced within the shower. The energy deposition in the electromagnetic shower is dominated by ionization losses of electrons in the material, which is also approximately proportional to the total track length. It follows, that the number of Cherenkov photons is then proportional to the deposited energy [14]. The Cherenkov light is detected by photon detectors: i.e. by Photomultiplier Tubes (PMTs) or Multi-pixel Avalanche Photo Diodes (MAPDs). The charge of the PMT pulse is then also directly proportional to the deposited energy.

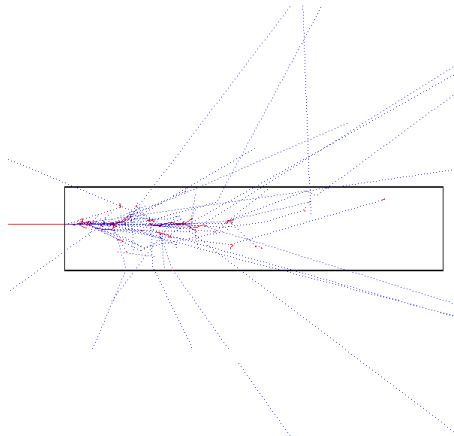
A very important parameter of a calorimeter is its energy resolution, which is defined as:

$$\left(\frac{\sigma_E}{E}\right) = \left(\frac{a}{\sqrt{E}}\right) \cdot \left(\frac{b}{E}\right) \cdot (c), \quad (2.5)$$

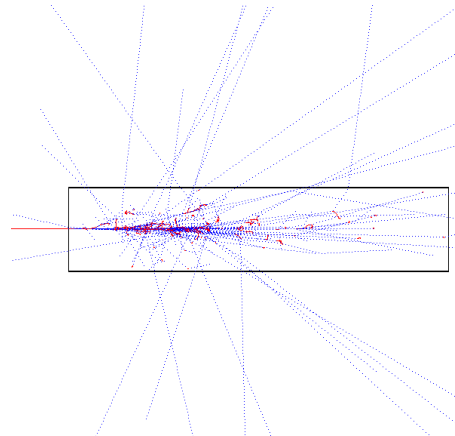
where a characterizes the photoelectron statistic (stochastic term), b characterizes the noise of the readout electronic and c characterizes the possible uncertainty in the calibration. For example, the OPAL lead glass modules which will be used for the HADES ECAL detector had an energy resolution of

$$\frac{\sigma_E}{E} = \frac{5\%}{\sqrt{E[\text{GeV}]}} \quad (2.6)$$

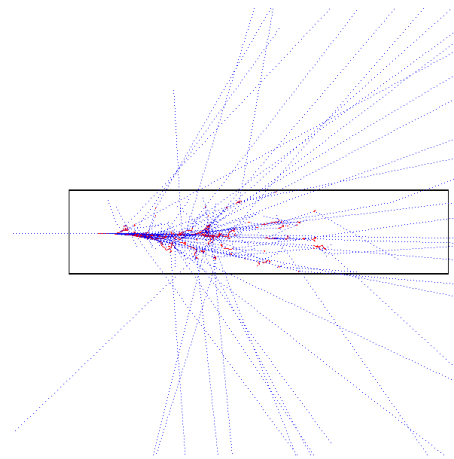
in which the stochastic term is dominant [15]. However, after several years of operation in a high radiation environment the energy resolution needs to be investigated again.



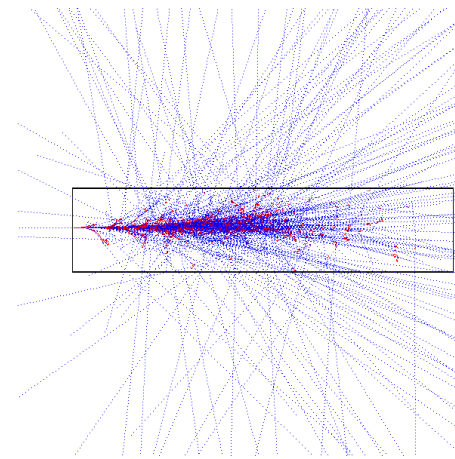
(a) Electron (500 MeV/c): electromagnetic (el. mag.) shower.



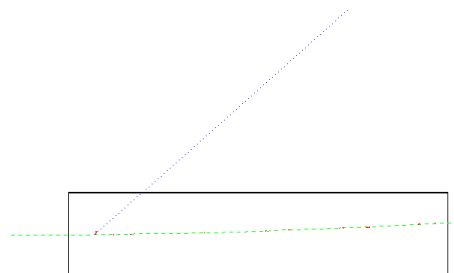
(b) Electron (1 GeV/c): increased shower size and intensity as compared to (a).



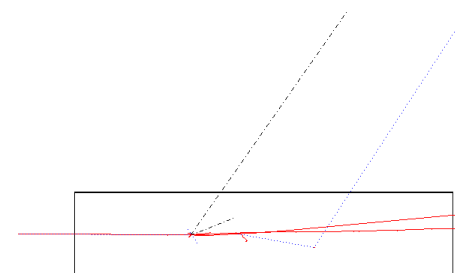
(c) γ (1 GeV/c): el. mag. interaction, similar to (b).



(d) γ (5 GeV/c): high intensity el. mag. shower.



(e) Muon (2 GeV/c): no strong interaction, no el. mag. shower.



(f) Proton (2 GeV/c): no el. mag. shower, neutrons and protons kicked out via strong interaction.

Figure 2.3: HGeant2 Monte Carlo simulation [19] of a lead glass module of the HADES ECAL detector for different incoming particles with different momentum. The incoming particles hit the lead glass module perpendicular from the left. Cherenkov light, which is produced in all cases is not displayed in this simulation. Secondary produced particles are shown: $e^{-/+}$: red, γ : dashed blue, μ : dashed green, p: red, n: punctured-dashed black.

After an appropriate energy calibration one can measure the energy of fully absorbed particles. Later, in beam measurements require monitoring of each individual module. To detect module failure and drifts, one could for example insert pulsed LED light into the calorimeter modules and measure the response of the detector to these pulses.

2.2 General calorimeter read out techniques: Photomultiplier Tubes (PMTs) and Multi-pixel Avalanche Photo Diodes (MAPDs)

In high energy physics mainly photosensors used, based on the internal photoelectric effect (i.e. photodiodes based on semiconductor technology) or the external photoelectric effect (i.e. photomultiplier tubes), in order to detect the emitted light in the range from ultraviolet (UV) up to near infrared (IR). In the following the physics of Photomultiplier Tubes (PMTs) and Multi-pixel Avalanche Photo Diodes (MAPDs) is illustrated. In particular common technical challenges and problems for PMTs are discussed.

Today, the photomultiplier tube remains unequalled in light detection. The advantages of PMTs stems from the following features:

- large sensing area,
- fast response and excellent timing performance,
- high gain and low noise.

The last two give a PMT an outstanding high gain and band width product. A disadvantage is the cast for the PMT and the high voltage supply.

2.2.1 The Photomultiplier Tube (PMT) and common technical problems and challenges

A *Photomultiplier Tube* (PMT) is a device to detect photons (with wavelength from ultraviolet (UV) up to near infrared (IR)) and convert them into a measurable electrical signal. The elements of a PMT are shown in Fig. 2.4. A PMT consists of an evacuated glass tube with a light sensitive photocathode behind the faceplate. The photocathodes normally used in PMTs are made of a deposited photoemissive semiconductors. Incoming photons can knock out electrons because of the external photoelectric effect. The photoelectrons are directed by the electric field of a focussing electrode to the first dynode of the electron multiplier. The purpose of the electron-optical input system is to focus all the photoelectrons onto the area of the first dynode. The ratio between the number of electrons reaching the first dynode and the total number of electrons emitted by the photocathode is called the collection efficiency. It should be greater than 80%. Last but not least, the transit time of electrons between the photocathode and the first dynode should be independent of their initial velocity and point of origin. The electron multiplier consists of several stages of dynodes, with a high voltage applied, to accelerate the electrons and produce secondary electrons on the next dynode. The dynodes are arranged such that the electric field between them cause the electrons emitted by each dynode to strike the next with an energy of a few hundred electronvolts. In this way the number of electrons grows from dynode to dynode and gives the required

multiplication (called gain) of typically 6 orders of magnitude. The signal of one or more incoming photons is amplified in such a way and an output signal can be measured. A schematic view of the working principle of a linear focused PMT is shown in Fig. 2.4.

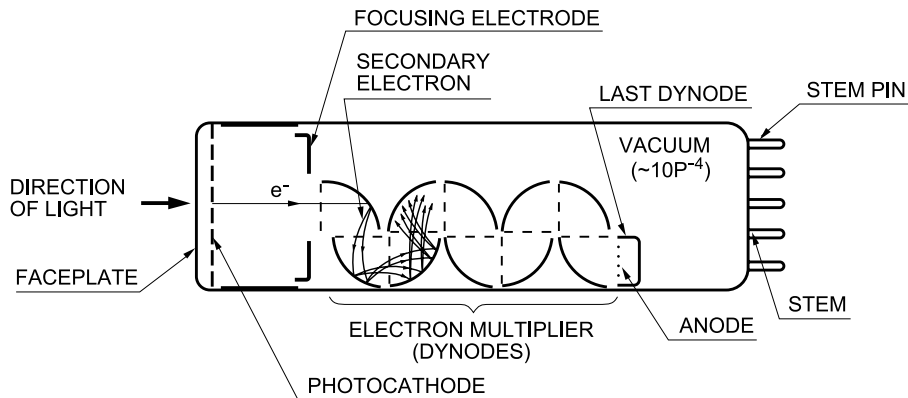


Figure 2.4: Working principle of a linear focused Photomultiplier Tube (PMT). The two phenomena fundamental to the operation of a PMT are photo emission on the photocathode and secondary electron emission at the dynodes [17].

Spurious pulses

In addition to the main pulse, which is created as explained above, so-called spurious pulses can be observed. These pulses are caused by two main effects, namely: luminous reactions and ionisation of residual gas.

Luminous reactions are reactions when the dynodes are bombarded by electrons with emission of photons. These, so called afterpulses, can be observed 20 - 100 ns after the main pulse [22]. This time delay is caused by the sum of the light and electron transit times in the PMT. It is also possible that a photon passes the photocathode and releases a photo effect directly on a dynode. This leads to so called prepulses. One can observe them several nanoseconds before the main pulse 2.5.

The other type of afterpulses is caused by ionisation of residual gas in the vacuum tube. Because of the slowly accelerated gas ions one can observe this pulses 100 - 3000 ns after the main pulse [22]. The different effects leading to pre- and afterpulses are schematically shown in Fig. 2.5.

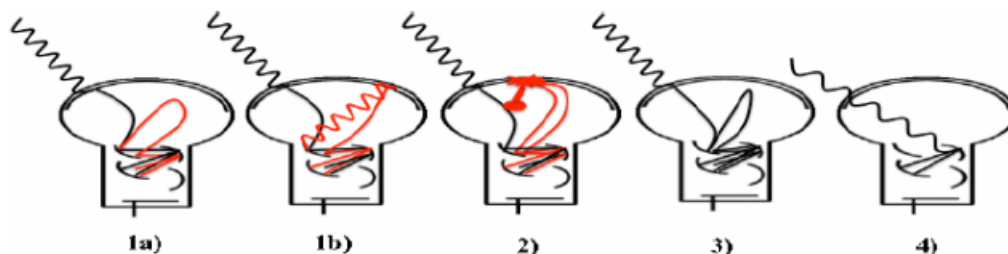


Figure 2.5: Different effects leading to pre- or afterpulses: Afterpulses of type 1, due to escaped e^- (1a) or due to escaped γ (1b). Afterpulses of type 2, due to ionisation of residual gas. Late pulses type 3, due to e^- reflection. Prepulses type 4, caused by photo effect on the dynode. [7]

Influence of magnetic fields

Magnetic fields, even as weak as the earth magnetic field, can affect the performance of photomultiplier tubes. PMTs are very sensitive to magnetic field because the trajectories of the electrons could be bended out of the multiplication region. Changing the orientation of a PMT in the earth's magnetic field (in Central Europe the values are: $44 \mu\text{T}$ vertical component, $20 \mu\text{T}$ horizontal component [8]) can show a detectable effect. In order to reduce this effect PMTs are often shielded by a material with high magnetic permeability, so called Mu-metal. The output variation between a magnetic unshielded and a magnetic shielded PMT, exposed to a magnetic field from different directions, is shown in Fig. 2.6. The magnetic field sensitivity is measured relative to three perpendicular axes (see 2.6, right panel).

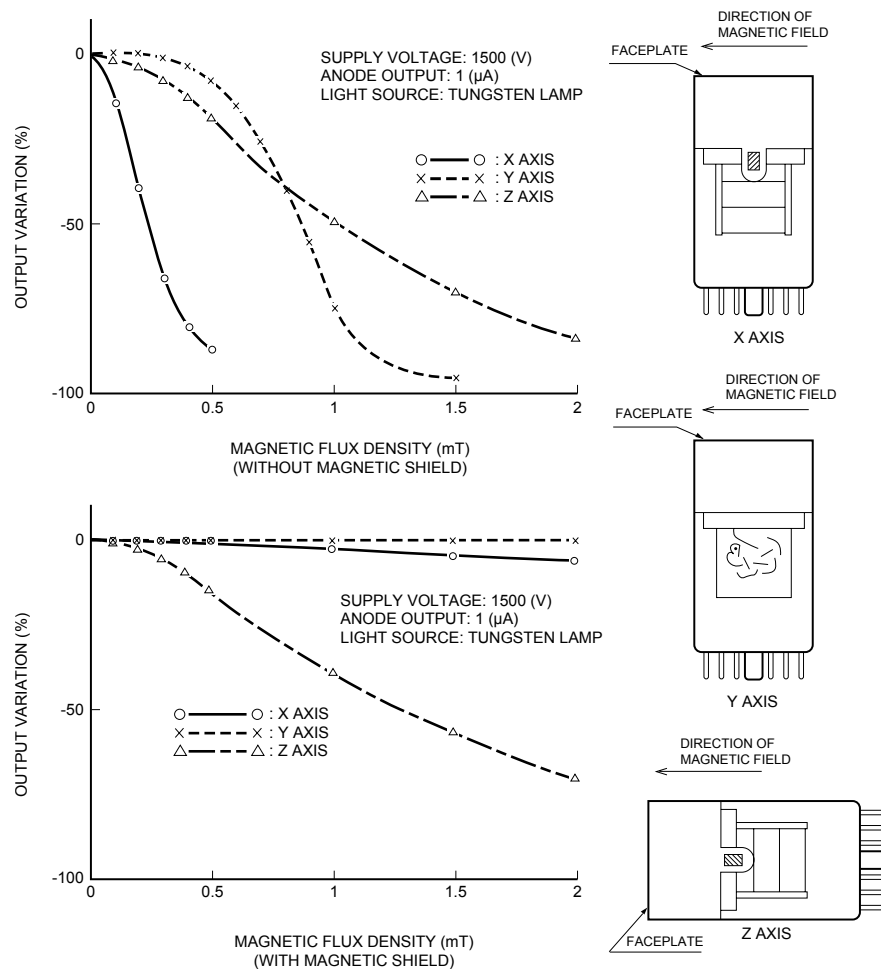


Figure 2.6: The output gain variation between a magnetic unshielded and a shielded PMT exposed to a magnetic field from different directions as a function of magnetic field. Upper panel: without magnetic shield; lower panel: with magnetic shield [17].

Uniformity of light collection

The photocathode sensitivity of a PMT can be measured, for example by scanning the faceplate diagonal with a perpendicular light beam with 1 mm diameter. The relative output of a PMT for

such a scan is shown in Fig. 2.7. Higher sensitivity at the border regions of the photocathode can be observed. A possible explanation is the fact that light reflected from internal electrodes gives the reflected photons one more chance to strike the photocathode [22].

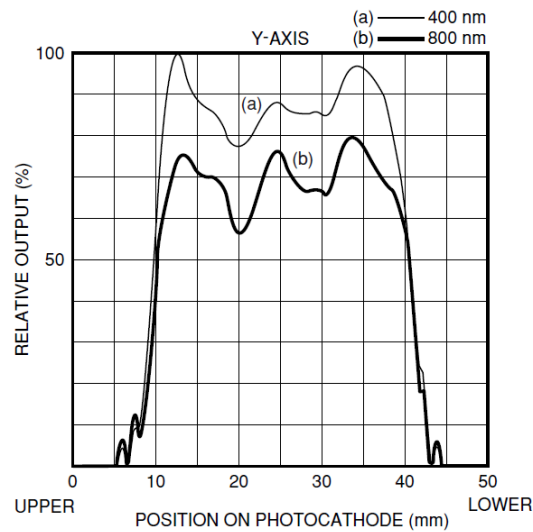


Figure 2.7: The relative output of a PMT by scanning its photocathode with a 1 mm light beam with different wavelength. Higher output can be measured at boarder regions [17].

Radiation

Ionizing radiation can give rise to secondary effects such as dark current noise increases or if the radiation is sufficiently intense, permanent loss of sensitivity and gain.

Temperature

Photomultiplier tubes are also sensitive to temperature variations because of the nature of their photosensitive and secondary electrons emitting materials. The gain dependence on temperature amounts to typically 0.7% per degree [24]. Thus, a stable gain requires temperature control.

2.2.2 The Multi-pixel Avalanche Photo Diode (MAPD)

A *Multi-pixel Avalanche Photo Diode* (MAPD) is based on semiconductor technology and is also a device to detect weak light signals. It is built of many pixels of *avalanche photodiodes* (APDs). The working principle of a typical APD is shown in Fig. 2.8 (left panel). Incoming photons pass through the silicon dioxide layer and the negatively doped **n**-region and positively doped **p**-region up to the depletion region (neutral charge area). In this region photons can excite free electrons and holes, called carriers or electron-hole pairs. The electrons migrate to the anode and the holes to the cathode. A reverse bias-voltage is applied to accelerate the carriers. The carriers will collide with the crystal lattice, ionization takes place and new electron-hole pairs are generated, just like a chain reaction. This phenomenon is called avalanche multiplication.

An APD is mostly used in Geiger mode. This means that the diode is operated slightly above the breakdown threshold voltage, where a single electron-hole pair can induce a strong avalanche. A big advantage of APDs is that they can operate without problems in high magnetic fields.

MAPDs have an excellent photon counting capability. If a MAPD is irradiated with low intensity light and connected to an amplifier, discrete pulse height variations according to the number of detected photons can be observed. Fig. 2.8 (right panel) shows an overlap display of pulse waveforms visible on an oscilloscope. The pulse heights are clearly separated for different numbers of incident photons.

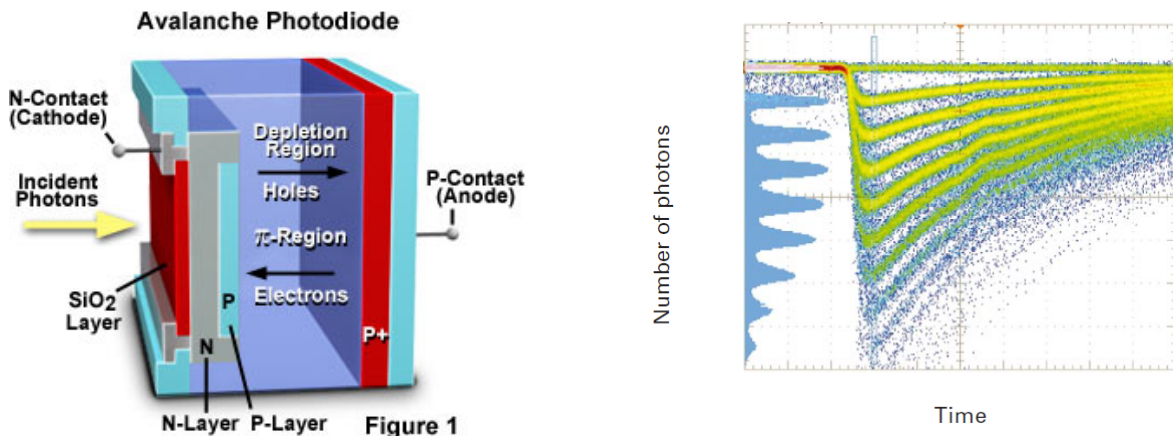


Figure 2.8: Left: Components and working principle of an Avalanche Photo Diode (APD) [18]. Right: Overlap display of pulse waveforms visible on a oscilloscope when using an amplifier. The MAPD is irradiated with low intensity light. Pulse height variations according to the number of detected photons can be observed [18].

2.3 HADES ECAL module properties

Each HADES ECAL module consists of a modified lead glass module obtained on loan from the OPAL experiment at CERN [25][15]. Lead glass (Corning CEREN 25) is used as a Cherenkov radiator. The glass has a density of $\rho = 4.06 \frac{\text{g}}{\text{cm}^3}$, a refraction index of $n = 1.708$ (at 410 nm) and a radiation length of $X_0 = 2.51 \text{ cm}$. All modules have the same length of 420 mm (16.7 radiation lengths). The transverse size of $92 \times 92 \text{ mm}^2$ is comparable to the transverse size of the expected electromagnetic showers (see Fig. 2.3). A brass box with a thickness of 0.45 mm is used as a housing for the module and the PMT and its high voltage divider (HV-divider). For detection of the Cherenkov light a PMT is connected to one side of the lead glass block via optical grease (RHODORSIL Paste No. 7). All sides of the block are mirror polished and wrapped in white paper (Tyvek[®]) to reduce lateral escape of photons. An optical fibre is coupled to the lead glass block with a standard optical link connector on the end plate to open the possibility to put external LED light into the module. A schematic view and the photograph of a disassembled module is shown in Fig. 2.9.

Up to now there are several considerations for different PMTs with photo cathode sizes ranging from 1 up to 3 inch. Tests were done using a 1.5 inch EMI 9903KB, 1 inch HAMAMATSU R8619 (with HV-divider H10580) and 3 inch HAMAMATSU R6091 (with tapered HV-divider H6559)

PMTs. Both pulsed LED light and cosmic muons are used as sources for the on-going test and they are subject of this work. Preliminary results of these investigations are shown in section 4.

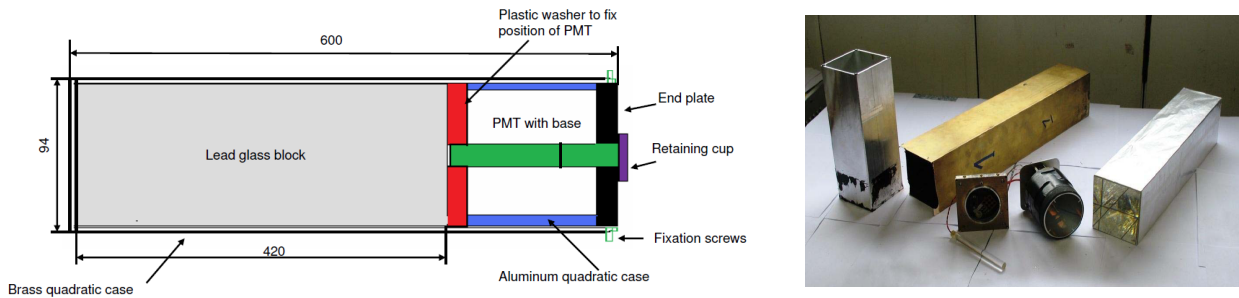


Figure 2.9: Left: A schematic view of an ECAL calorimeter module with its components [9]. Right: A disassembled ECAL module. One can identify the brass housing (left side), the lead glass block (right side), the high voltage divider and the PMT (middle) [9].

2.4 CBM PSD module properties

The PSD detector will be a modular lead-scintillator sampling calorimeter with a good and uniform energy resolution. It will be built of 44 individual modules, each consisting of 60 lead/scintillator layers covering a surface of $20 \times 20 \text{ cm}^2$. The light of each scintillator will be collected by wavelength shifting (WLS) fibres. The read out will be done by MAPDs with an active area of $3 \times 3 \text{ mm}^2$ and a pixel density of $10^4 / \text{mm}^2$. At the moment MAPDs (MAPD-3N) of the company Zecotek are below investigation [30]. A 3D model of a PSD detector module and photography of a PSD module prototype is shown in Fig. 2.10.

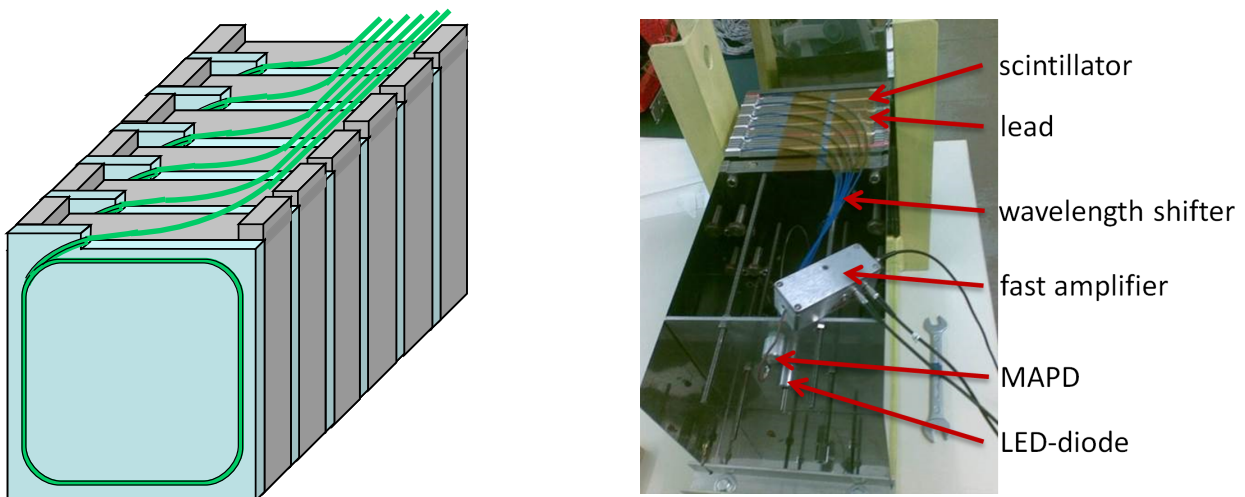


Figure 2.10: Left: A sketch of a PSD prototype module. The lead/scintillator layers (gray/blue) and the wavelength shifting (WLS) fibres (green) are visible [30]. Right: A PSD prototype with explanation of the different parts [30].

3 The COME and KISS read-out concept

In modern physics experiments analogue data generated by detectors require digitisation to get important information as time, amplitude and charge of an electric signal pulse. This information is essential to interpret nuclear physics experiments. *Application Specific Integrated Circuits* (ASICs) are common and very fast tools for digitalization of detector data. However, they are very expensive in the development. Current developments in *Field Programmable Gate Arrays* (FPGAs) open a new door to use them also for data digitalization. For example, time measurement, signal discrimination, amplitude digitisation (ADC) or charge digitisation (QDC) can be already done using an FPGA [29]. A major advantage of FPGAs is that they have a high quality circuit design and the development packages are documented in great detail.

The idea of the “COME and KISS” read-out concept is to use *commercial elements* (in this case a commercial FPGA) and the design and handling should be true to the slogan “*keep it small and simple*”. For calorimeters the charge of PMT or MAPD pulses are an important observable. In this case a charge digitisation in a commercial FPGA should be realized. For this purpose the charge is converted into a width measurement (Q2W) and the FPGA is used for time digitisation which is already implemented with very good time resolution [28]. The internal LVDS receivers of the FPGA will be used as discriminators. Small and simple electronic (resistors and capacitors) will be used to attenuate or amplify and integrate the detector raw signal.

For very fast detectors this concept has been realized by a group working with diamond detectors. The VIP-QM research group will focus on the optimization of this read-out electronics for calorimeters to achieve individually optimized time and energy measurements. The proposed design of read-out electronics for time and energy analysis by the “Grand Unified Readout“ team is shown in Fig. 3.1. The scheme can be used for a wide range of applications by tuning the amplifier characteristics.

3.1 The COME and KISS read-out concept for the ECAL detector in HADES

As discussed in detail in section 2.3, PMTs will be used for the HADES ECAL detector and require a dedicated read-out. Two read-out options are considered and will be described in the following.

3.1.1 HADES ECAL read-out requirements and general read-out scheme

The read-out chain of the HADES ECAL detector can be split into three main parts, namely: the front-end electronic, the trigger and read-out board and the data acquisition.

The front-end electronics

Up to now there are two options of front-end electronics considered. One is based on an ADC add-on card, designed for the HADES Pre-SHOWER detector, which is read out and digitised by the *General Purpose Trigger and Readout Board - version 2* (TRBv2) [11]. A prototype of this front-end board provides 8 channels with separated outputs for time and amplitude measurements. The SHOWER add-on board operating at 20 MHz with 10 bit resolution is used as an ADC. A HPTDC (High Performance general purpose Time-to-Digital-Converter) based on the TRBv2 is used as a Time-to-Digital-Converter (TDC). Three front-end board prototypes were designed and manufactured at the Smoluchowski Institute of Physics of Jagellonian University of Cracow. Tests were performed at GSI Helmholtzzentrum für Schwerionenforschung in Darmstadt and are still ongoing. The energy resolution for pulser signals, similar to PMT signals, have been measured to be about 1% and a time resolution less than 100 ps could be achieved [9].

The other option is based on a charge-to-width (Q2W) conversion implemented in an FPGA. The basis of this board is the already existing PaDiWa (PandaDircWasa) TDC front-end board. The new Q2W front-end board, called PaDiWa AMPS, is an extension of the PaDiWa3 board and now under construction [27] and will be ready to be tested in October 2013. This board will be read out by the *General Purpose Trigger and Readout Board - version 3* (TRBv3) [13] developed at GSI Helmholtzzentrum in Darmstadt. The detailed characterisation of this option is under investigation and are subject of this work. A detailed description can be found in sections 3.1.2 and 3.1.3.

The trigger and read-out board

As digitizing board the *General Purpose Trigger and Readout Board - version 3* (TRBv3) [13] is foreseen. The TRBv3 is a multi purpose time digitisation board with high resolution (23 ps RMS [13]) Time-to-Digital Converters (TDC) realized in FPGAs (Lattice ECP3-150EA). The board can handle up to 256 channels and is equipped with a DAQ functionality, with fast data transfer via gigabit Ethernet. A major advantage of this multi-purpose digitisation board is that it is easy to operate and it has a well-documented “plug and play” functionality.

The data acquisition (DAQ)

After digitizing, the data is combined to HADES-sub-events and is sent to the HADES-DAQ system via optical links. The TrbNet protocol will be used for Level-1-Trigger (LVL1) distribution and data collection, as well as for slow control. Data is then transported to the event-builders via gigabit Ethernet. It is foreseen to use the HADES-DAQ system, which can be adapted for the HADES ECAL detector.

3.1.2 COME and KISS charge-to-width (Q2W) measurement with an FPGA - the PaDiWa AMPS front-end board

The duty of the read-out electronic will be to get time and charge information of primary (so called raw) data from (calorimeter) detectors. The charge can be obtained by a charge-to-width measurement with the help of an FPGA. A Charge-to-Digital-Converter (QDC) based on a modified Wilkinson ADC [23] will be implemented in an FPGA. The analogue input signal is integrated by a capacitor, which is afterwards discharged linearly, via a discriminator triggered current source. The time needed to discharge the capacitor is measured by a TDC, implemented in an FPGA. This time is proportional to the integrated charge. For accuracy it is important to keep the baseline rather constant. A better accuracy of charge measurement compared to a resistor–capacitor-discharge (RC-discharge) can be achieved by a fast crossing of the threshold (see section 4.7.1). In addition, this method of discharging a capacitor works as an automatic baseline restorer, since a charge equivalent to the input charge is injected with opposite sign.

The working principle and signal chain of the COME and KISS charge measurement (Q2W) with the help of an FPGA is schematically shown in Fig. 3.1. The KISS part (1) is an attenuator/amplifier system made of discrete electronics. The signal is then split into a fast and an integrated signal. The fast signal is processed in a charge to width conversion system (2) implemented mainly in an FPGA. The last part is the time digitisation circuit (3) which consists of two branches and is also implemented in an FPGA. The first branch is for the fast signal and for timing and the second one for a pulse width measurement which encodes the charge. Thus, two channels are needed for one input channel.

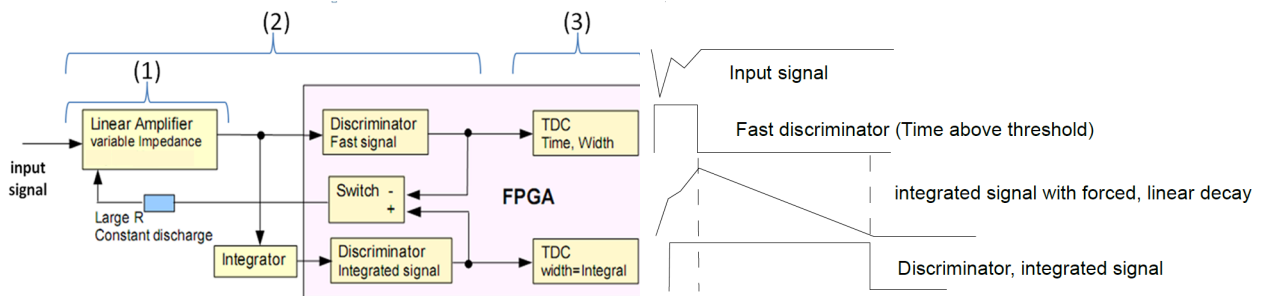


Figure 3.1: Sketch (left) and schematic signal chain (right) of the COME and KISS charge measurement (Q2W) with an FPGA. The KISS part (1) is an attenuator/amplifier system made of discrete electronics. The signal is then split into a fast and an integrated signal. The fast signal is processed in a charge to width conversion system (2) implemented mainly in an FPGA which is the COME part. The last part is the time digitisation circuit (3) which consists of two branches and is also carried out in an FPGA. One is for timing via the fast signal and the other one for a pulse width measurement, which encodes the charge. [20].

A four channel prototype with discrete components (transistor, op-amp, discriminator) based on this concept has been already developed and successfully tested with a pulse generator. First test

results of this prototype are shown in Fig. 3.2. After a walk correction a charge resolution of 0.17% has been achieved [29].

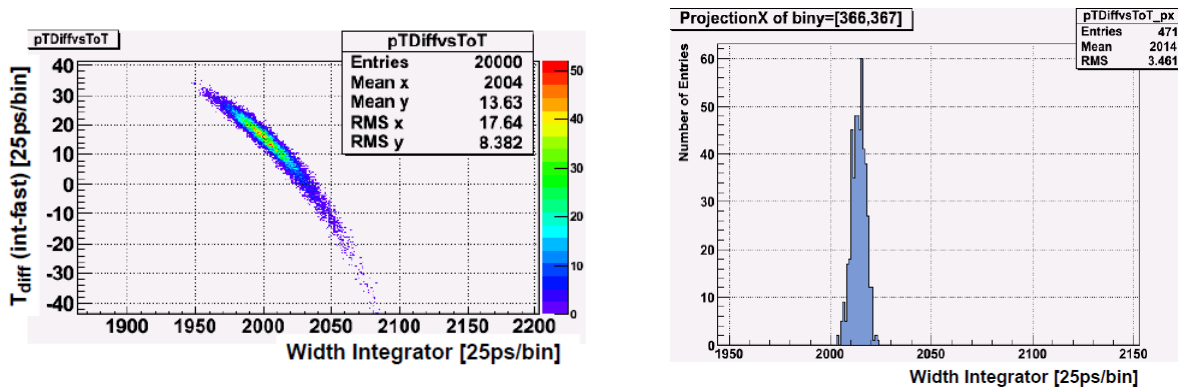


Figure 3.2: First test results of a four channel prototype with discrete components. Left: The width measurement via the linear discharge of the integrated pulser signal (horizontal axis). Time difference between the leading edges of the fast and the integrated signal showing a clear correlation with the jitter of the measured width (vertical axis). The width measurement of the pulser signal in a multi-hit TDC. Right: The intrinsic charge resolution of 0.17% which can be achieved after a walk correction procedure based on the correlation shown in the left figure [29].

A new prototype based on the PaDiWa3 front-end board, called PaDiWa AMPS, is now in a production stage. This front-end board can be controlled and read out by the TRBv3. The layout of the PaDiWa AMPS front-end board is shown in Fig. 3.3.

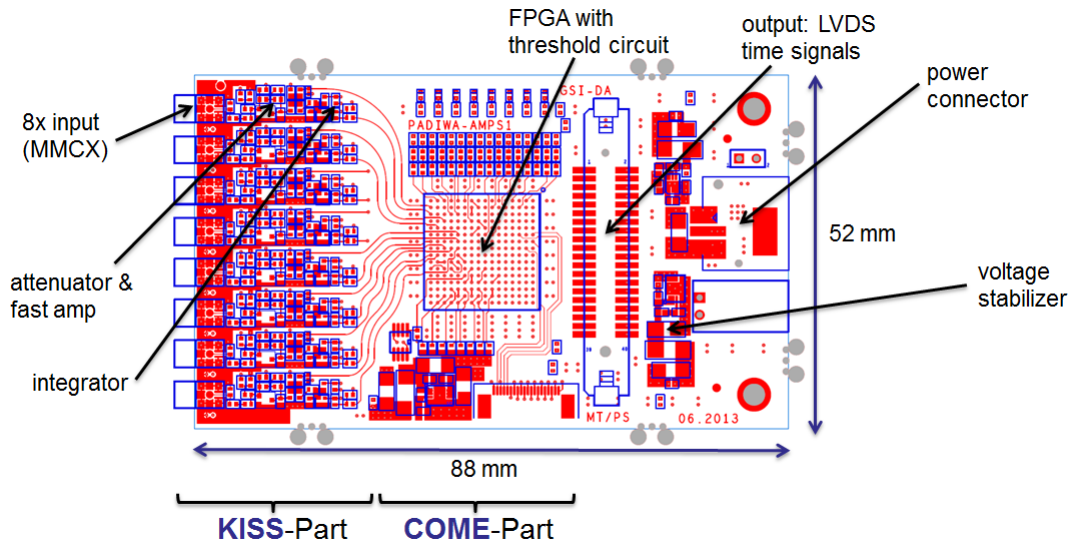


Figure 3.3: Layout of the prototype based on the PaDiWa3 front-end board called PaDiWa AMPS, which is now under development [20].

3.1.3 State-of-the-art simulations of the Q2W-electronics

Simulations with the program SPICE (Simulation Program with Integrated Circuit Emphasis) were done [20], to check the integrity of the circuit design and predict circuit behaviour of the PaDiWa

AMPS board. As input a signal shape which is similar to those from a 1 GeV gamma ray detected by a PMT was used. Fig. 3.4 shows the input signal, the result of the fast amplifier and integrator with nearly constant decay slope. A calibration curve for the charge (energy) to width (time over threshold) is also shown in Fig. 3.4. It shows a large dynamic range of 250.

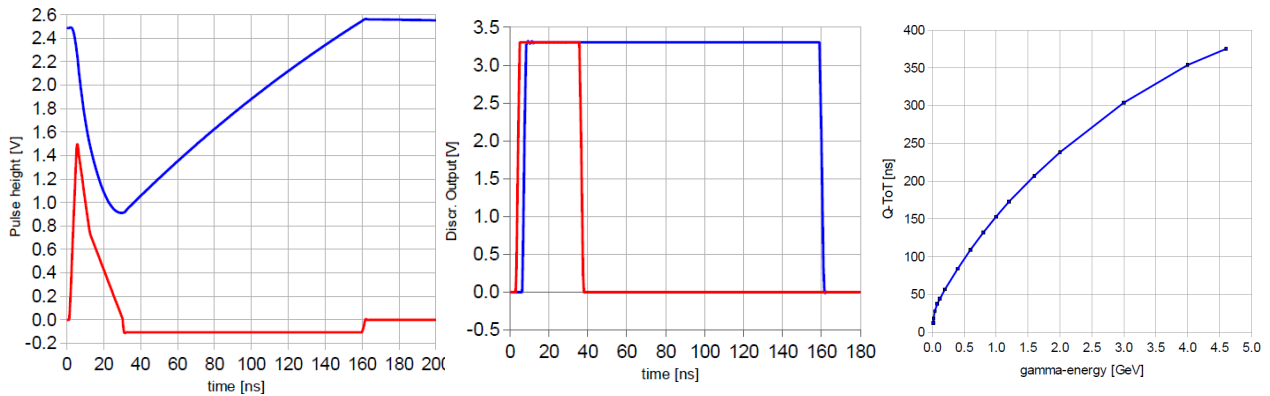
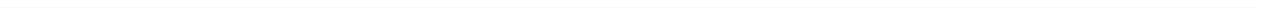


Figure 3.4: Left: Simulation results of the fast amplifier and integrator with constant decay slope. Analogue signal after liner amplification (red) and after integration (blue) for a PMT signal from a 1 GeV gamma ray (schematic shape) is shown. Middle: Discriminator output for the fast (red) and the integrated (blue) signal. Right: Calibration curve for the charge (energy) to width (time over threshold). It shows a large dynamic range of 250 [20].

3.2 Possible applications of the COME and KISS readout concept

In the recently developed concept both, time and energy digitisation, is done within an FPGA in real time. Data is transferred to mass storage and slow control is performed via ETRAX processors running Linux and based on a 100 Mbit/s Ethernet interface. Since this is a general concept it is of interest for a wide range of applications. Not only detectors (calorimeter type) read out by photomultiplier, where the focus could be on achieving additionally energy resolution could benefit from it. For example a pixelated diamond sensor could be combined with a very fast read-out being capable of handling rates up to a few times 10^6 per pixel. Finally, detectors like e.g. drift chambers could also benefit from this read out concept.



4 First COME and KISS measurements

It is important to understand raw pulse shapes and the response of a detector, to adapt the readout electronic optimally to it. At the test set-up at the GSI Helmholtzzentrum für Schwerionenforschung different calorimeter type detectors are available. A HADES ECAL module test set-up with different PMT types and a prototype of the PSD detector for the CBM experiment, which is read out by a MAPD was assembled in the GSI detector laboratory. The detector response of both calorimeters can be tested by pulsed LED light and with cosmic muons triggered by a coincidence measurement with plastic scintillators. To get reference results for readout electronics a commercial oscilloscope (RS 1044) was used.

4.1 Installation of a test set-up to characterize calorimeter type detectors and their readout electronics

A new test stand in the detector hall at the GSI Helmholtzzentrum für Schwerionenforschung in Darmstadt was set-up to characterise calorimeter type detectors and their readout electronics. Laboratory devices have been commissioned and calibrated for the first time. A HADES ECAL module support structure was built and set up. A PMT test-box was constructed to test the characteristics of PMTs. A TRBv3 with a PaDiWa1 front-end electronic was installed. Fig. 4.1 depicts the new test set-up.



Figure 4.1: The new test set-up to characterize calorimeter type detectors and their readout electronics at GSI Helmholtzzentrum für Schwerionenforschung in Darmstadt. Left: computer terminals, remote high voltage supplies; Middle: Calorimeter modules and support structure; Right: low voltage supplies, pulse generators, oscilloscope, TRBv3 readout board.

4.1.1 HADES ECAL test set-up

An important task for the future HADES ECAL detector measurements of the detector system response of each of the about 1000 lead glass modules with pulsed LED light or cosmic muons. Later measurements with a photon beam are intended. Modules with different PMTs are available and the aim is to find a PMT which meets all the requirements.

PMT test-box

A light tight PMT test-box was build based on a standard polypropylene pipe to adapt a 3 inch HAMAMATSU R6091 PMT. This allows performance and characteristic tests of single PMTs. Three holes with 1 mm diameter, located from the centre of the faceplate to the edge, enable the possibility to test the PMT with a pulsed standard blue LED. A photography of this test-box is shown in Fig. 4.2. It is foreseen to build also a PMT test-box for the 1 inch HAMAMATSU R8619 PMT.

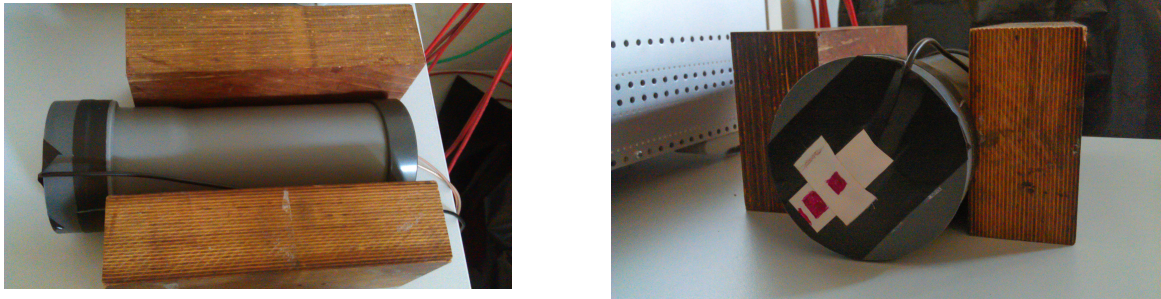


Figure 4.2: Top (left) and front (right) view of the PMT test-box, which allows to characterise 3 inch HAMAMATSU R6091 PMT with LED light.

HADES ECAL module support structure

A support structure for up to four ECAL modules was build from item[®] aluminium profiles. It allows to test the modules, in vertical position (pointing upwards) with cosmic muons, triggered by an upper and lower plastic scintillator. The plastic scintillators are read out by PMTs. For the coincidence measurement of both scintillators a Constant-Fraction Discriminator (CF8000) and a Quad coincidence Nim module are used to provide a trigger signal. A disassembled plastic scintillator with its PMT is shown in Fig. 4.4. The dimensions of the plastic scintillator is $80 \times 80 \text{ mm}^2$ (This is smaller than the lead glass dimensions of $92 \times 92 \text{ mm}^2$). A photograph of the support structure for ECAL modules and a schematic view of the ECAL module set-up for cosmic muon measurements are shown in Fig. 4.3.

It is also possible to put pulsed LED light into the ECAL modules. For that a standard blue LED is connected to an optical fibre. This fibre can be easily plugged into the module via a standard optical link connector. A light distribution system to test more modules with the same LED is currently under development [9].

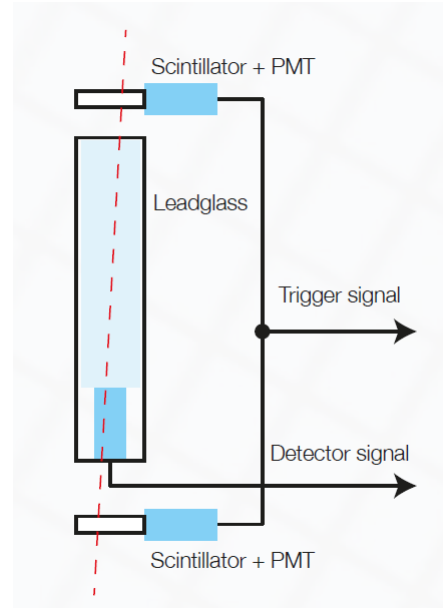
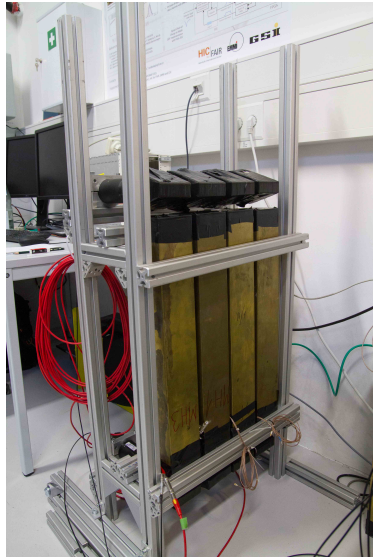


Figure 4.3: Left: Support structure, which allows the test of up to four ECAL modules simultaneously in a vertical position. Right: Sketch of a ECAL module set-up for measurements with cosmic muons [16].

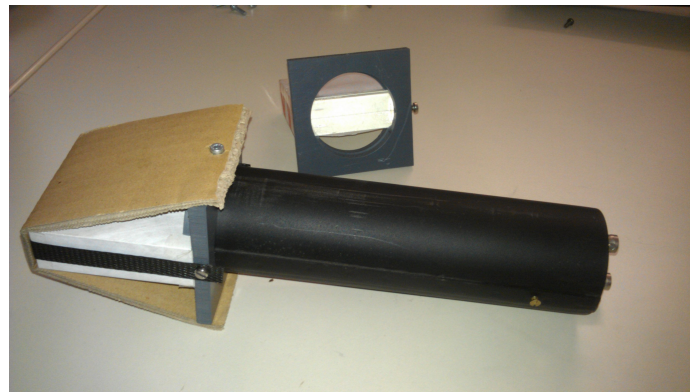


Figure 4.4: Photography of a scintillation trigger used to trigger cosmic muons. One can identify the plastic scintillator, warped in paper (Tyvek[®]), which is mounted to a PMT (HAMAMATSU H1949).

4.1.2 CBM PSD test set-up

A prototype of the PSD detector for the CBM experiment is available at the new test set-up as well. The prototype can be tested by pulsed LED light or by cosmic muons. For that a trigger scintillator coincident measurement, similar to the cosmic muon trigger used for the HADES ECAL modules can be used. In Fig. 4.5 a sketch of the PSD prototype is shown.

4.1.3 PaDiWa + TRBv3 test set-up

To characterise the front-end electronics described in section 3, a TRBv3 was installed with a PaDiWa front-end board. With this board first investigations of the FPGA (which will also be used

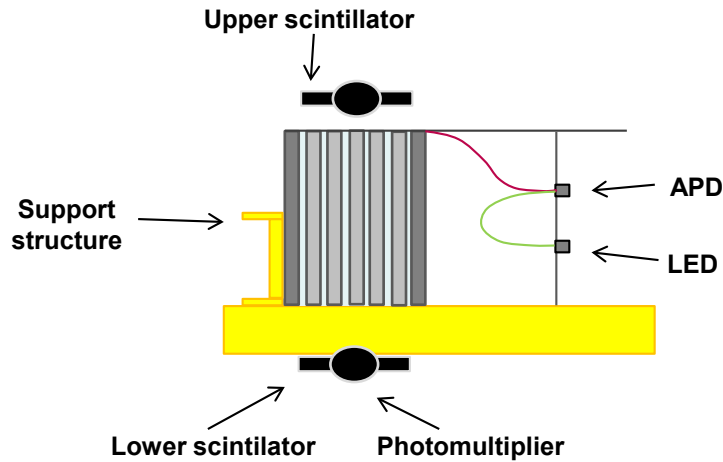


Figure 4.5: Sketch of the PSD prototype for the CBM experiment. Scintillation light is transmitted via WLS fibres to a MAPD. It can be tested with cosmic muons, by a coincidence measurement similar as used for HADES ECAL modules or with pulsed LED light [30]. For details see also section 2.4.

on the PaDiWa AMPS front-end board) can be done. Also the DAQ system of the TRBv3 can be tested with this set-up.

4.2 KISS measurements with a commercial oscilloscope

A modified COME and KISS readout concept was used to characterise the response of HADES ECAL modules and the CBM PSD detector prototype. A commercial oscilloscope (RS 1044), in a small and simple set-up, was used as a “reference” readout electronic and data acquisition (DAQ). To improve the readout resolution, raw signals were shaped by tools provided by the oscilloscope. Investigations were done, to optimize the readout concept and to estimate its resolution. Also a first proof of principle of the high quality of this readout concept will be shown by means of the PSD prototype for the CBM experiment.

4.2.1 The readout principle and its intrinsic resolution

In the following measurements the oscilloscope was not used in “standard” mode. A pulse shaping by tools of the oscilloscope was used, to integrate the detector signals. An analogue 20 MHz bandwidth filter was adapted before signal digitisation to shape the signal. After digitization a DSP-filter (digital signal processing filter) with a cut-off frequency of typically $f_{\text{DSP-cut-off}} = 10 \text{ MHz}$ (low pass filter) was used. The typical signal chain of the used oscilloscope is shown in Fig. 4.6. By using this filter set-up, the input pulse is shaped (Gaussian shape) and its amplitude is reduced by a factor of about 2.5 (depending on the primary pulse shape). This configuration equals to a weighted moving average with a full width half maximum (FWHM) of about $\frac{1}{f_{\text{DSP-cut-off}}}$ as integration/shaping time and is a method to integrate/shape the signal. In Fig. 4.7 the difference between a pulser raw signal and the shaped signal is shown.

To show that this settings improves the readout resolution, investigations with a pulser were performed. Different filter settings were used and an amplitude/minimum measurement of a

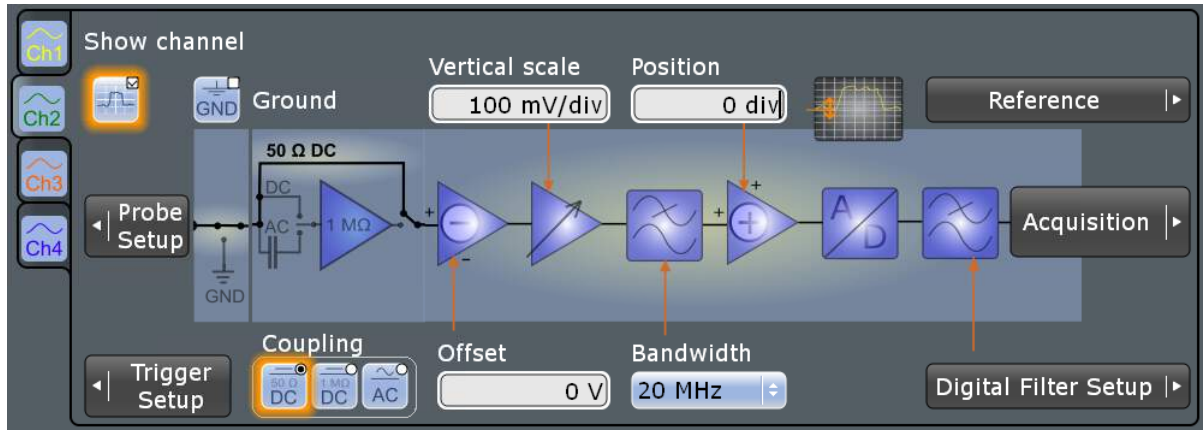


Figure 4.6: Typical signal chain of the used oscilloscope (RS 1044). The bandwidth filters can be placed before digitisation. The cut-off frequency of the DSP-filter $f_{\text{DSP-cut-off}}$ can be set after the digitisation, in the Digital Filter Setup menu.

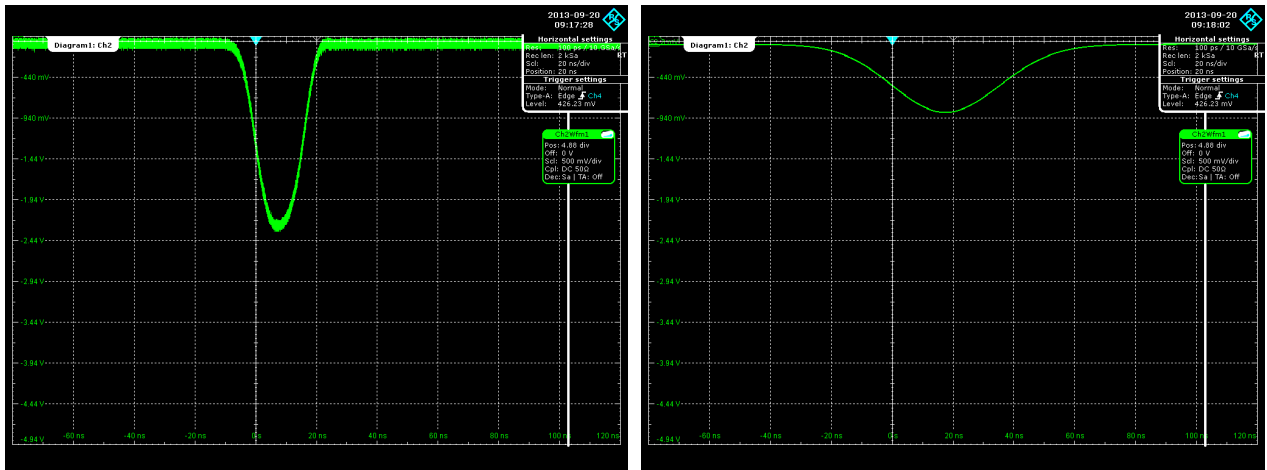


Figure 4.7: Left: Raw pulser signal as it is displayed on the oscilloscope with full bandwidth. Right: The same pulser signal, but now shaped by using an analogue 20 MHz bandwidth filter and a DSP-filter with a cut-off at $f_{\text{DSP-cut-off}} = 20 \text{ MHz}$.

negative pulser signal (frequency: 1.1 kHz, amplitude: 2.36 Vpp, leading-/trailing-time: 8.4 ns, width: 16 ns) was performed via the oscilloscope. A typical amplitude/minimum measurement, performed by the oscilloscope, is shown in Fig. 4.9. The intrinsic electronics (plus pulser) resolution can be calculated by σ/mean , where these values were measured by the oscilloscope. In Fig. 4.8 the resolution for different filter settings are shown. The resolution of a standard 8-bit DAQ can be estimated from the binning $1/256 = 0.39\%$ of the full scale. A resolution of about 0.5% could be measured for the raw pulser signal, without filter settings on the oscilloscope. By using a digital filter set-up with an analogue 20 MHz bandwidth filter and a DSP-filter with a cut-off at 20 MHz, the resolution can be significantly decreased to values below 0.1%. By applying too low cut-off frequencies (integrating over longer times than the signal base width) the resolution deteriorates. This can be explained, because now the noise on the baseline is also integrated, which leads to larger sigma's.

High measuring rates can be achieved by pulser measurements. The statistical error, calculated by $1/\sqrt{N}$, is for more than 10000 measurements below 0.1%. Because of that the statistic error will be neglected in the following pulser measurements.

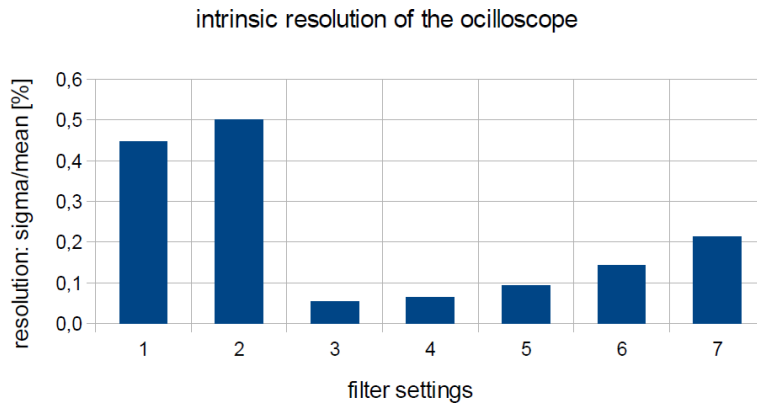


Figure 4.8: The intrinsic resolution (sigma/mean) of the used oscilloscope (RS 1044) was characterised by a minimum measurement of a negative pulser signal. Different digital filter settings were used: 1) full bandwidth, 2) 20 MHz bandwidth filter, 3) 20 MHz bandwidth + 20 MHz DSP-cut-off filter, 4) 20 MHz bandwidth + 10 MHz DSP-cut-off filter, 5) 20 MHz bandwidth + 5 MHz DSP-cut-off filter, 6) 20 MHz bandwidth + 3 MHz DSP-cut-off filter, 7) 20 MHz bandwidth + 2 MHz DSP-cut-off filter.

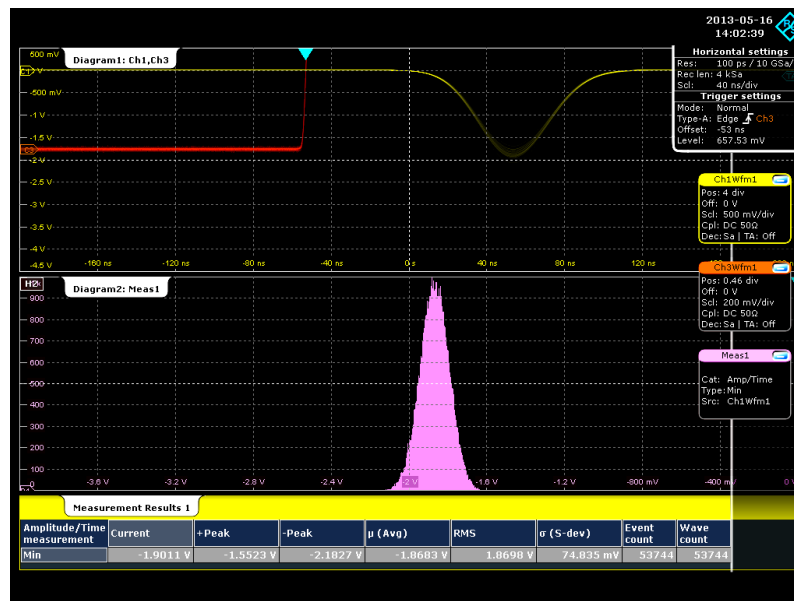


Figure 4.9: Typical amplitude/minimum measurement. The minimum of a negative shaped signal (yellow) is measured and the results are shown in the measurement result box (table on the bottom). It is also possible to log the measured results in a histogram (magenta).

4.2.2 Proof of principle: readout electronics resolution and single photo electron peaks from a MAPD

Photon counting is an effective technique used to detect light. When the electron content of a single photon pulse in a channel reaches a certain level the channel saturates. It is possible to use this as an advantage by operating under saturation conditions to reduce gain fluctuations significantly. This opens the possibility to detect very low current pulses (photon counting) with i.e. a MAPD.

To finally show that an oscilloscope can be used as a “reference” readout electronics and DAQ system, the PSD detector from the CBM experiment was used. Pulsed LED light (frequency: 10 kHz, amplitude: variable, leading-/trailing-time: 8.4 ns, width: 16 ns) was sent into the detector. The response of the MAPD (Zecotec MAPD-3N), operated at a bias-voltage of 91 V, was analysed with an oscilloscope. A dedicated fast amplifier, developed by the Institute for Nuclear Research in Moscow, was used to amplify the MAPD signal. The raw pulse shapes of the detector are noisy, primary caused by high frequency noise of the MAPD. The signal was shaped by the oscilloscope (20 MHz bandwidth filter and DSP-filter cut-off at 10 MHz). A pulse height measurement of the shaped signal was performed (as described in section 4.2) and the values were recorded into a histogram. The data of the histogram can be saved into a .csv file, for later analyses with ROOT (a Data Analysis Framework based on C++, developed at CERN). In Fig. 4.10 the result of such an amplitude measurement in comparison to a standard charge measurement done without pulse shaping is shown. Up to 8 single photo electron peaks, corresponding to the photoelectrons detected with the MAPD, can be clearly separated.

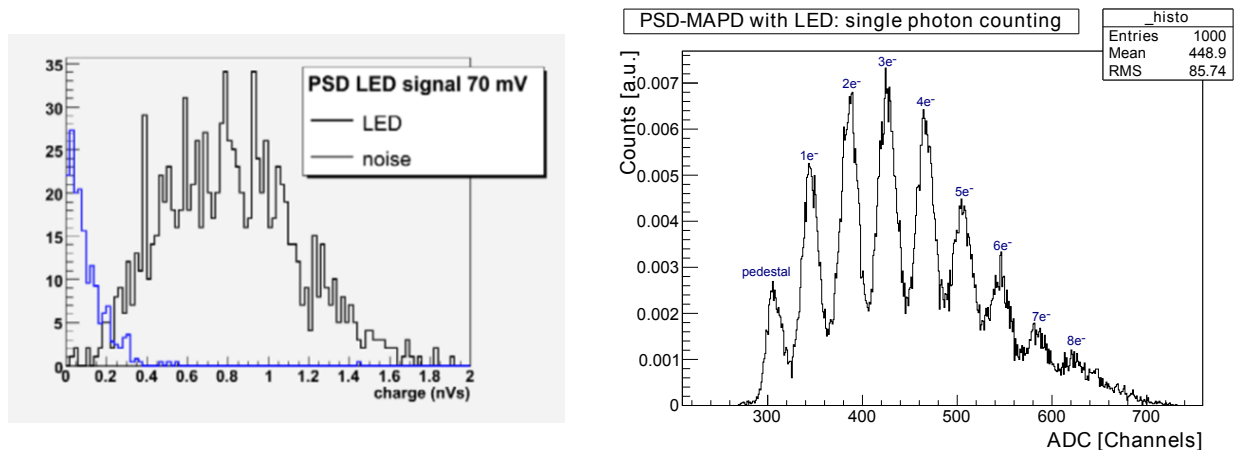


Figure 4.10: Left: Charge measurement done without pulse shaping of a MAPD driven by LED light of low intensity [26]. Right: Pulse height measurement of a MAPD, which is driven by LED light of low intensity. The signal was shaped by the digital filter of the oscilloscope. Up to eight photo electron peaks can be clearly separated.

It has been shown, that an oscilloscope can be used as “reference” readout electronic. By applying digital filters, the intrinsic resolution could reach about 0.1%. Calorimeter type detectors can be characterised by this readout method.

4.3 Characterisation of HADES ECAL PMTs

It is an important task to understand the pulse shapes of the PMTs, used in the HADES ECAL detector, in order to adapt readout electronics optimally to them. In Fig. 4.11 raw pulse shapes of ECAL modules equipped with a 1 inch HAMAMATSU R8619 (left panel) and a 3 inch HAMAMATSU R6091 PMT (right panel) are shown for cosmic muons. Evidently the trailing-edge of the signal is very spiky. For the readout electronics it is important to understand the nature of this spikes. Pulse shapes of the 3 inch HAMAMATSU R6091 PMT were analysed. Tests of gain stability, uniformity of light detection and the dependence of the earth magnetic field were performed. For the following measurements the test-box described in section 4.1.1 was used. Results of these investigations and a discussion of the nature of this spikes are shown in the next section.

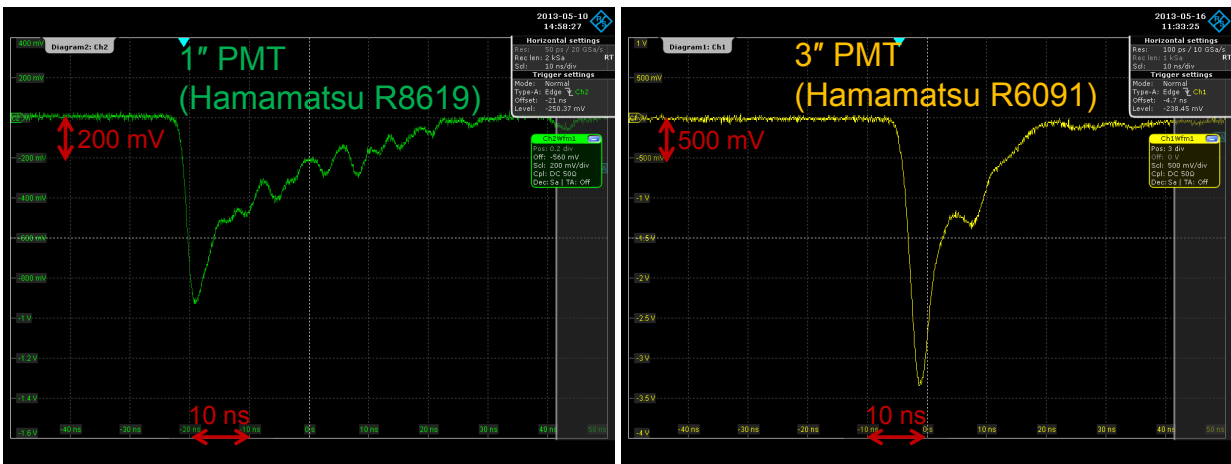


Figure 4.11: Raw pulse shapes for cosmic muons of ECAL modules equipped with a 1 inch HAMAMATSU R8619 (left) and 3 inch HAMAMATSU R6091 PMT (right).

4.3.1 Identification of spurious pulses in 3 inch HAMAMATSU R6091 PMTs

As it has been discussed in section 2.4 spurious pulses can be found in PMT pulse shapes. To identify them, pulse shapes of a 3 inch HAMAMATSU R6091 PMT in a test-box and the same model in a HADES ECAL module were analysed and compared. Pulsed LED light and cosmic muons were used as test signals.

To find spurious pulses, both, LED light (frequency: 110 Hz, leading-/trailing-time: 8.4 ns, width: 16 ns) was inserted into the test-box and an ECAL Module, to produce PMT output signals of about 1 V. The PMTs were powered with a supply voltage of 1500 V. In both PMT signals one could observe prepulses with an amplitude of about 10 - 15 mV about 10 - 20 ns before the main pulse appears (see Fig. 4.13). As explained in section 2.2.1 these pulses are probably caused by photons passing the photocathode and making a photoelectric effect on the first dynode. Afterpulses, probably due to luminous reactions, could also be observed about 50 - 80 ns after the main pulse (see Fig. 4.13). An accumulation of several pulse shapes measured with the test-box and the ECAL module PMT set-up is shown in Fig. 4.14 (left panel). In the accumulated pulse spectrum a

conspicuous peak with an amplitude of about 20 mV can be observed about 350 ns after the main pulse. This peak corresponds to He⁺ or H⁺ ions which are slowly accelerated to a dynode.

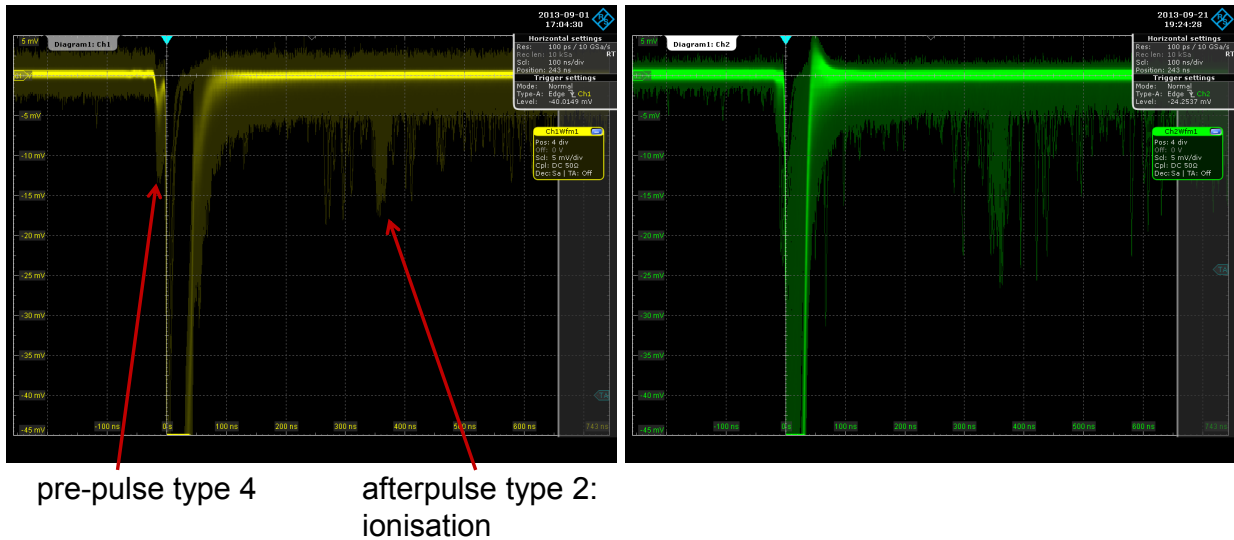


Figure 4.12: Accumulation of several pulse shapes of a 3 inch HAMAMATSU R6091 PMT (at 1500 V). The PMT output amplitude is 1 V. Prepulses of type 4 can be observed 20 - 30 ns before the main pulse (see section 2.2.1). A conspicuous peak due to of ionisation effects can be observed about 350 ns after the main pulse. Both spurious pulse types can be observed in pulse shapes of a PMT in the test-box (left) and the module (right).

In Fig. 4.14 an accumulation of pulse shapes of a 3 inch HAMAMATSU R6091 PMT in the test-box (left panel) and the same PMT model in a ECAL module (right panel) is shown. The pulses were generated by cosmic muons, in the lead glass and by photons induced by ionising radiation for the PMT in the test-box. Signals with an amplitude of about 300 mV were triggered by the oscilloscope. By comparing the trailing-edges of a PMT signal in the test-box with a PMT signal in an ECAL module, a characteristic spike, about 5 ns after the main pulse, can be observed. The estimation in equation 4.1 shows that 5 ns corresponds to a path length of Cherenkov light in lead glass of about 0.9 m. This is about two times the lead glass length. In Fig. 4.11 (right) a PMT signal for a cosmic muon passing the module in axis from up to down is shown. In this pulse shapes a characteristic spike about 8 ns after the main pulse can be observed. In general one can say that these spikes, which can be observed 5 - 8 ns after the main pulse are probably caused by reflections of Cherenkov light in the module. The reflection of Cherenkov light in the module seems to be a complicated process, strongly influenced by a total reflection capability of the photons which depends on emission angles. Further verification of this effect is on-going.

$$\frac{c_0}{1.708} \cdot 5 \text{ ns} = 0.88 \text{ m} \quad (4.1)$$

In the case of the HADES ECAL detector prepulses in PMT signals (see Fig. 4.13 and 4.14) can result in completely wrong information about the arrival time of the particles, if the signal threshold is set too low. This will destroy the matching of time-of-flight measurement by the RPC detector in front of the ECAL detector. The result would be, that the contamination of electromagnetic

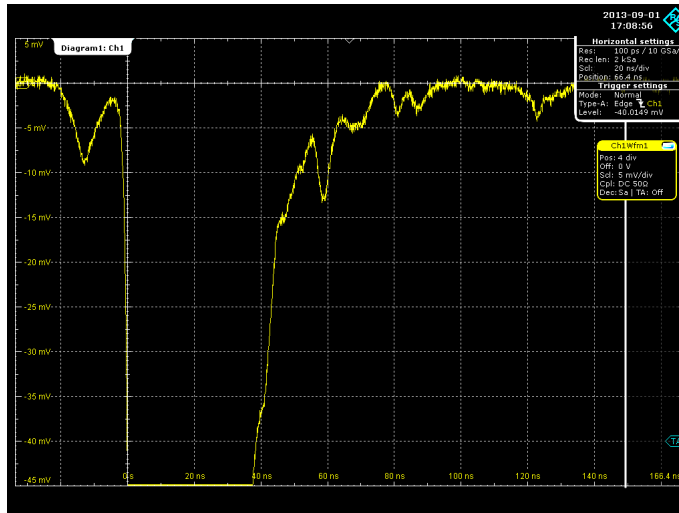


Figure 4.13: Zoom into a pulse shape of a 3 inch HAMAMATSU R6091 PMT (at 1500 V) in the test-box driven by a LED. The PMT output amplitude is 1 V. A prepulse of type 4 can be observed about 10 ns before the main pulse (see section 2.2.1). Afterpulses probably caused by luminous reactions are visible 40-100 ns after the main pulse.

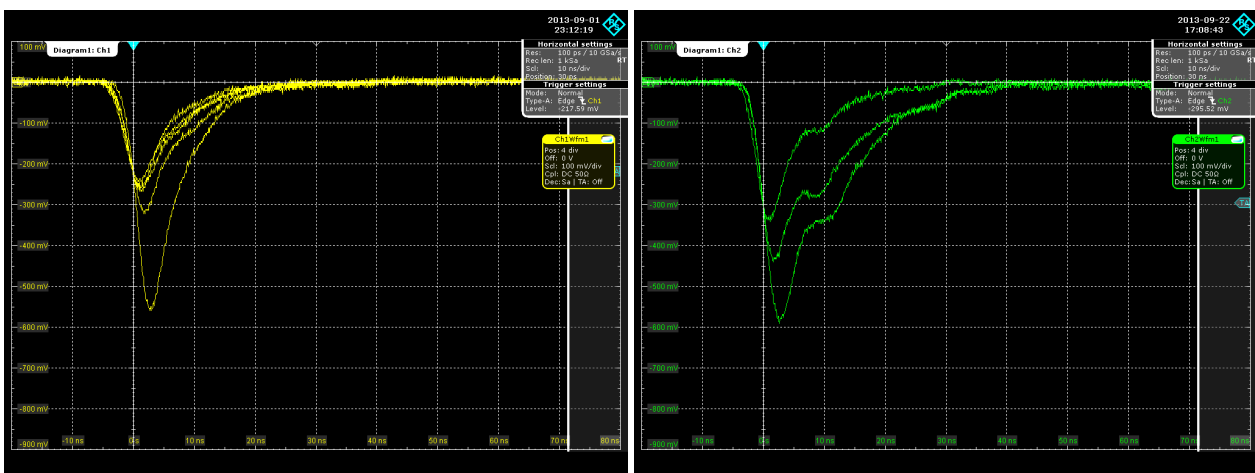


Figure 4.14: Accumulation of pulse shapes of a 3 inch HAMAMATSU R6091 PMT (at 1500 V) in the test-box for photons induced by ionising radiation (left) and the same model in an ECAL module for cosmic muons (right). In the pulse shape of the ECAL module PMT a characteristic spike about 5 ns after the main pulse is visible. This spike probably corresponds to reflections of Cherenkov light in the module which is not emitted directly towards the PMT.

showers, due to the large amount of protons and pions can not be corrected for. Furthermore the timing signal of the ECAL detector is needed to discriminate against slow neutrons which strongly interact with the lead glass. A shift towards shorter time-of-flight times by several nanoseconds would destroy this discrimination power. On the other hand the threshold needs to be low enough to cover the large dynamic range, needed to cover the physics cases of interest. Since at PMT pulse heights of 1 V nearly all prepulses have an amplitudes below 10 mV (see Fig. 4.14), a dynamic signal range of 100 can be achieved.

In Fig. 4.15 a PMT pulse shape of a 1 inch Hamamatsu R8619 PMT in an ECAL module for cosmic muons is shown. The trailing-edge looks spiky. A possible explanation of this signal shape are multiple reflection of Cherenkov light in the module not entering the small active area of the PMT directly, but also ringing effects of the HV-divider cannot be excluded. Deeper investigations of this PMT are on-going, test-box measurements are foreseen.

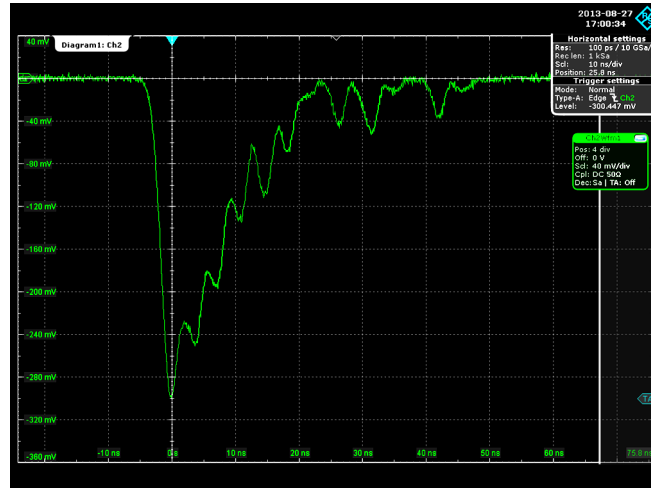


Figure 4.15: Typical pulse shape of a 1 inch Hamamatsu R8619 PMT (at 1500 V) in a ECAL module for cosmic muons.

4.3.2 Amplitude/gain stability of 3 inch HAMAMATSU R6091 PMTs

The amplitude/gain stability of a 3 inch Hamamatsu R6091 PMT in the test-box was monitored for 16 hours. During this time a PMT was fed with pulsed LED light (frequency: 110 Hz, leading-/trailing-edge: 8.4 ns, width: 16 ns) just in the middle of the test-box. With the help of an oscilloscope, an amplitude measurement as explained in subsection 4.2 was performed (20 MHz analogue bandwidth filter and DSP-filter cut-off at 10 MHz). Every 60 s the averaged results were logged into a histogram. In Fig. 4.16 the measured amplitude as a function of time is shown. As one can see the PMT needs about 120 minutes until stable working conditions are reached. This indicates a settling time to reach thermal equilibrium (see section 2.4).

4.3.3 Uniformity of light collection of 3 inch HAMAMATSU R6091 PMTs

The uniformity of light collection of a 3 inch HAMAMATSU R6091 PMT in the test-box was studied. The PMT was powered with a supply voltage of 1500 V. Pulsed LED light (frequency: 110 Hz, leading-/trailing-edge: 8.4 ns, width: 16 ns) was sent through one of the holes (1 mm diameter) on the front plate of the test-box which was touching the faceplate of the PMT. The LED was moved from the center to the edge hole position and an amplitude measurement of the shaped (20 MHz analogue bandwidth filter and DSP-filter cut-off at 10 MHz) PMT signal, as explained in section 4.2, was performed. The result is shown in Fig. 4.17. The effect described in section 2.4, which shows

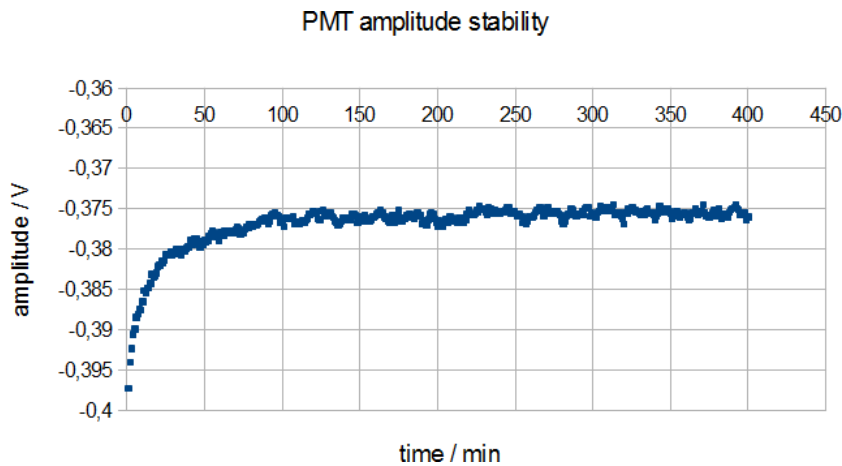


Figure 4.16: Mean values of an amplitude measurement, of the shaped PMT signal, as a function of time. Averaged values were stored into a histogram every minute. Stable working conditions are reached after about 120 min of running.

that PMTs can draw higher amplitudes/gain by collecting light at positions near to the borders of the photocathode, could be observed. A pulse height variation of up to 30% was found.

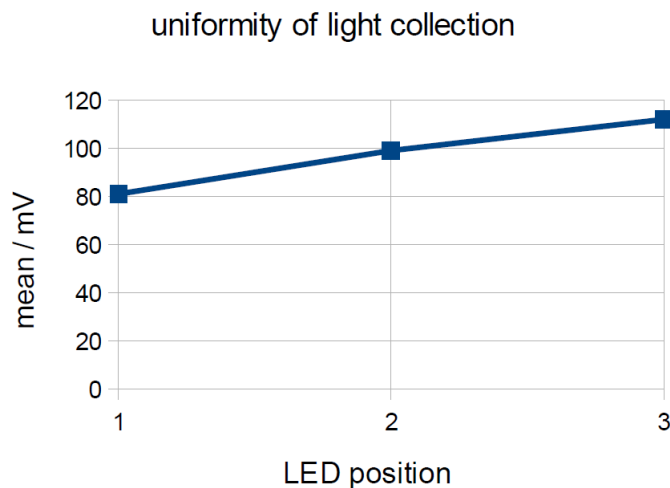


Figure 4.17: Mean value for an amplitude measurement of the shaped PMT pulse, for three LED positions (1: center position, 2: 1/2-, 3: 1/1 of the full radius of the active area of the PMT) of a 3 inch HAMAMATSU R6091 PMT.

4.3.4 (Earth) magnetic field influences on 3 inch HAMAMATSU R6091 PMTs

PMTs are very sensitive to magnetic field, as discussed in section 2.4. Strong magnetic fields may permanently magnetize some parts of a PMT, constantly affecting its performance. The dependence of the output amplitude/gain of a 3 inch HAMAMATSU R6091 PMT to the earth magnetic field could be observed by rotating the PMT and changing thereby its orientation with respect to earth magnetic field (electromagnetic leakage fields because of laboratory devices in the surrounding can not be fully excluded). The PMT in the test-box was illuminated with pulsed LED light (frequency: 110 Hz, leading-/trailing-edge: 8.4 ns, width: 16 ns). The photocathode of the PMT

was directed to West and South and a yaw- and roll-rotation was done. An illustration of the different orientations performed with an shielded PMT is shown in Fig. 4.18. An amplitude measurement of the shaped (20 MHz analogue bandwidth filter and DSP-filter cut-off at 10 MHz) pulse was performed for several orientations. This measurement was repeated with a shielded PMT. For that purpose the multiplication stage of the PMT was shielded with a tube of mu-metal (see Fig. 4.18). The measured PMT output amplitudes for the different rotations are shown in Fig. 4.19 and 4.20. By a roll rotation of 180°, a shift in the amplitude/gain of about 25% can be observed. Also a difference in the amplitude between the magnetic shielded and unshielded PMT could be observed, leading to higher amplitudes for the shielded PMT by up to 10%. Further investigations of these effects are on-going, in particular measurements with a full shielded PMT.

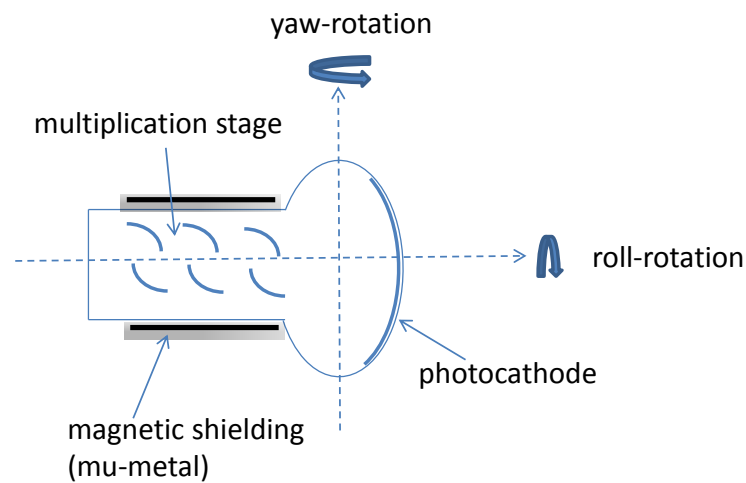


Figure 4.18: Illustration of yaw- and roll-rotation of a 3 inch HAMAMATSU R6091 PMT. The multiplication stage of the PMT can be shielded with a Mu-metal tube.

In the HADES ECAL detector the modules and thereby the PMTs are in a fixed position. The PMTs are calibrated taking into account all external effects and therefore the earth magnetic field would be not a severe problem. On the other hand, in order to optimise energy resolution. magnetic fields, including the earth's, to which a PMT is exposed have to be taken into account during the data calibration procedure and should be kept at a minimum.

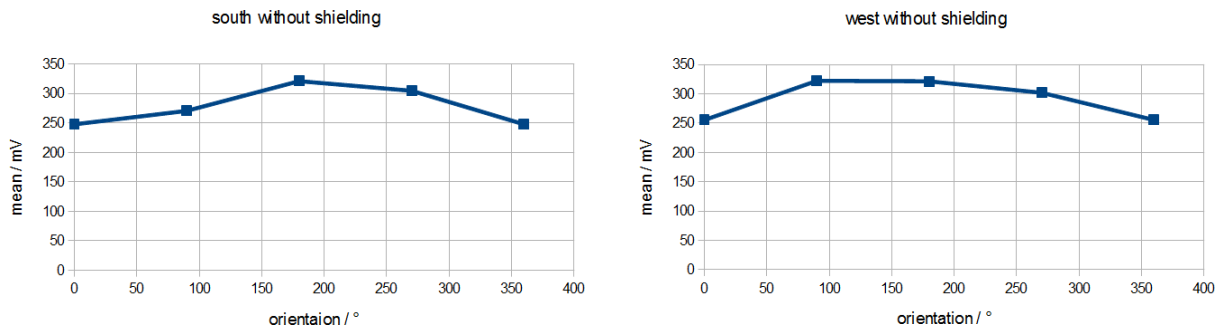


Figure 4.19: Mean value for a minimum measurement for a full roll rotation of an unshielded 3 inch HAMAMATSU R6091 PMT. The photocathode was directed to South (left) and West (right) directions.

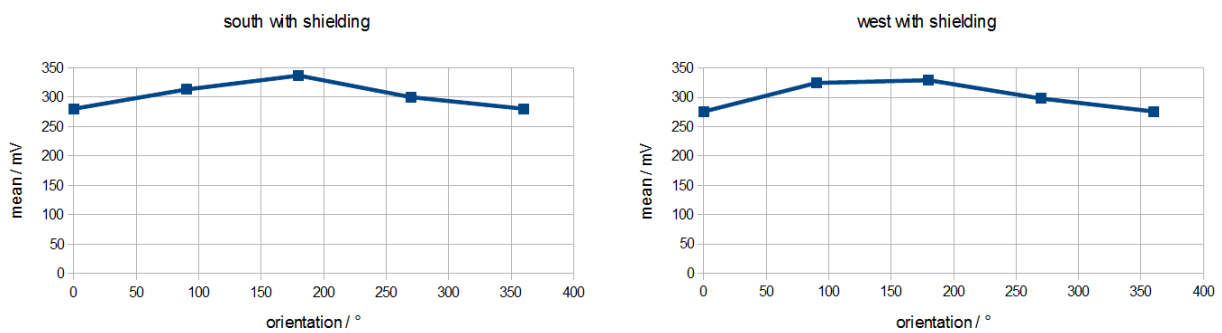


Figure 4.20: Mean value for a minimum measurement for a full roll rotation of a shielded 3 inch HAMAMATSU R6091 PMT. The photocathode was directed to South (left) and West (right) directions.

4.4 Determination of a lower boundary of the energy resolution of HADES ECAL modules

An oscilloscope (RS 1044) was used as a readout electronic and DAQ system to study the performance of full assembled ECAL modules with 1 and 3 inch PMTs. A pulse shaping as explained in section 4.2 was used. ECAL modules were investigated with pulsed LED light. Photon statistical effects were studied using two approaches. From the results a lower limit of the energy resolution of an ECAL modules equipped with a 3 inch HAMAMATSU R6091 PMT could be calculated. The same measurements were repeated for ECAL modules equipped with 1 inch HAMAMATSU R8619 PMTs.

4.4.1 Photon statistics limitation of ECAL modules resolution equipped with 3 inch HAMAMATSU R6091 PMT

The photostatistical characteristic of an ECAL module (module number: VH2) equipped with a 3 inch HAMAMATSU R6091 PMT was systematically studied by two approaches. Pulsed LED light (frequency: 1 kHz, width: 16 ns rise/fall-time: 8.4 ns, amplitude: with a variable) was inserted into the module (module number: VH2). The PMT was powered by a supply voltage of 2000 V.

first approach: width measurement to determine lower boundary on emitted photons via statistical fluctuations ($1/\sqrt{N}$)

For this approach the energy resolution was determined. Again an oscilloscope was used as readout electronics (see section 4.2) and an amplitude measurement of the shaped (20 MHz analogue bandwidth filter and DSP-filter cut-off at 10 MHz) signal was performed. The amplitude of the LED pulse was tuned to get a variable output amplitude of the PMT. For the different output amplitudes, the resolution was determined by a σ/mean ratio. In Fig. 4.21 (left) the result of this measurement is shown. At large pulse heights an energy resolution is found to be about or below 4%. Equation 4.2 shows, that for LED light the number of detected photons N can be estimated directly from the resolution. Fig. 4.21 (right) shows the result. A linear relation between pulse height and estimated photons is observed. By fitting these values with a straight line, the number of photons can be estimated by formula 4.3.

$$\text{resolution} = \sigma/\text{mean} = \frac{1}{\sqrt{N}} \Leftrightarrow N = \left(\frac{\text{mean}}{\sigma} \right)^2 \quad (4.2)$$

$$N_{\text{photons}} = 0.3335/\text{mV} \cdot \langle \text{PMT output (shaped)} \rangle - 1 \quad (4.3)$$

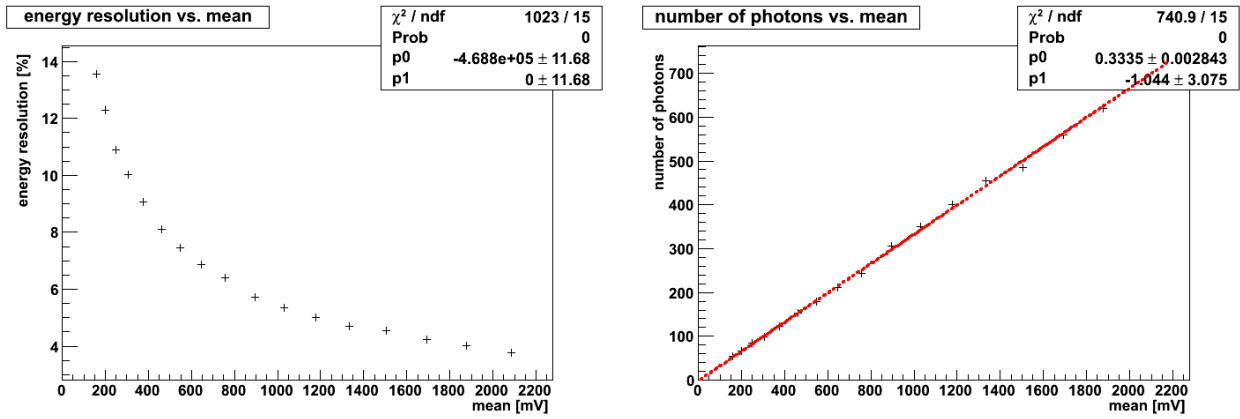


Figure 4.21: Left: Energy resolution as a function of the PMT output amplitudes for a module with a 3 inch HAMAMATSU R6091 PMT running at 2000 V driven by a LED. The expected energy resolution at an amplitude corresponding to cosmic muons (amplitude of about 1875 mV) is about 4% (see section 4.6). Right: The number of detected photons calculated for the different PMT output amplitudes via the photon statistical approach.

second approach: single photoelectron peak

Another approach to calculate the number of detected photons for a given signal amplitude can be performed via the single photoelectron peak of the PMT. A pulse height measurement of the shaped (20 MHz analogue bandwidth filter and DSP-filter cut-off at 10 MHz) signal was performed with the oscilloscope and the results stored into a histogram. The amplitude of the LED was reduced until the first photoelectron peak of the PMT was visible in the histogram. Because of triggering on the first electron peak the pedestal is cut away. The pedestal has to be found by a second measurement, by triggering randomly. The pedestal is shown in Fig. 4.22 (right). The position of the pedestal is needed to calibrate the histogram of the first photoelectron peak. The first photoelectron peak, which was calibrated by the pedestal, is shown in Fig 4.22 (left). By taking into account that one channel equals to 0.05 mV the first photoelectron peak equals to 2.365 mV (shaped signal). The estimated number of photons, for a given PMT pulse amplitude (shaped the same way), can now be calculated by the formula 4.4.

$$N_{photons} = \frac{\langle \text{PMT output (shaped)} \rangle}{2.365 \text{ mV}} \quad (4.4)$$

Photon statistic for ECAL modules with cosmic muons

Typical cosmic muons, measured with the same ECAL module and readout settings, have an amplitude of about 1875 mV (see section 4.6). From the first approach this value equals to $N_{photons} = 623 \pm 30$ photons and the expected energy resolution for this amplitude is about 4.0% (see Fig. 4.21). From the second approach one finds $N_{photons} = 793 \pm 40$ photons and a corresponding resolution $1/\sqrt{N}$ of 3.6%. By comparing these two results one can see, that additional effects contributes in the measured resolution. One of the effects is the position dependence

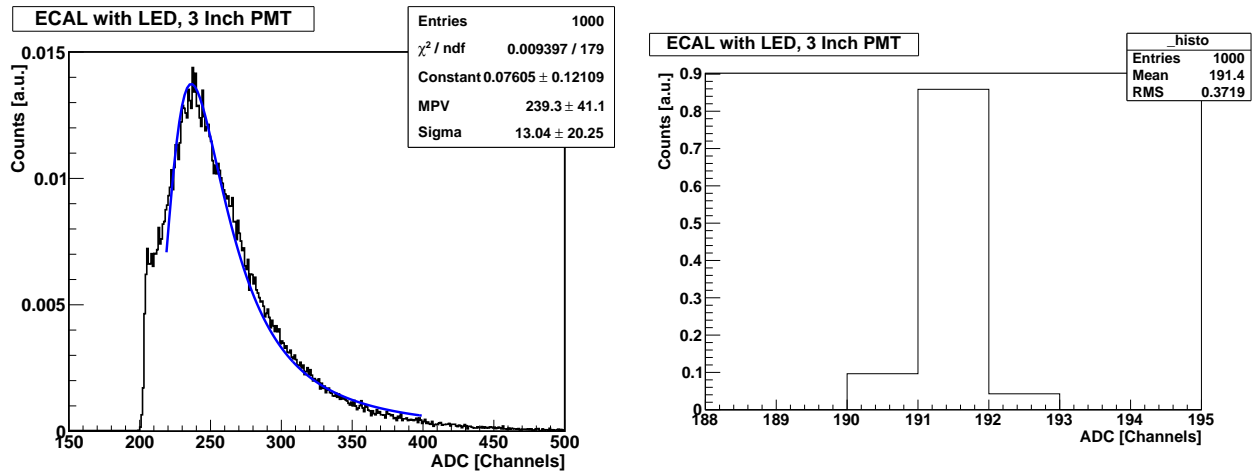


Figure 4.22: Left: Single photoelectron peak for a ECAL module equipped with a 3 inch HAMAMATSU R6091 PMT running at 2000 V driven by LED. The peak is described by a landau distribution. By calibrating with the pedestal (right) and taking into account that one channel equals 0.05 mV one can calculate the number of detected photons and thus, the contribution to the resolution given by photon statistics.

of the gain shown in Fig. 4.17, which adds to the signal fluctuation. In general the resolution determined by photon statistics via the single photo electron peak represents a lower limit and is found to be 3.6%.

4.5 Photon statistical properties of ECAL modules with 1 inch HAMAMATSU R8619 PMTs - gain non-linearity

The same measurements done for the first photon statistical approach in section 4.4, were repeated for a ECAL module (module number: MH3) equipped with a 1 inch HAMAMATSU R8619 PMT. The PMT was running at supply voltages of 1500 V and 950 V. The results are shown in Fig. 4.23. For PMT amplitudes higher than 120 mV (shaped signal) the relation between pulse height and estimated photons is not linear any longer. This is due to saturation effects of the PMT for pulses with high amplitude. It reflects a non-linearity in gain by running the PMT at too high supply voltages.

By looking to the characteristics of HAMAMATSU PMTs, a pulse linearity of $\pm 2\%$ (at 25 °C) up to 80 mA ($5 \text{ mA} \cdot 50 \Omega = 4000 \text{ mV}$) for the 3 inch HAMAMATSU R6091 PMT and up to 5 mA ($80 \text{ mA} \cdot 50 \Omega = 250 \text{ mV}$) for the 1 inch HAMAMATSU R8619 PMT can be found. As shown above, the 1 inch PMT shows saturation effect quite early, the 3 inch PMT is more rugged to higher amplitudes (see section 4.4).

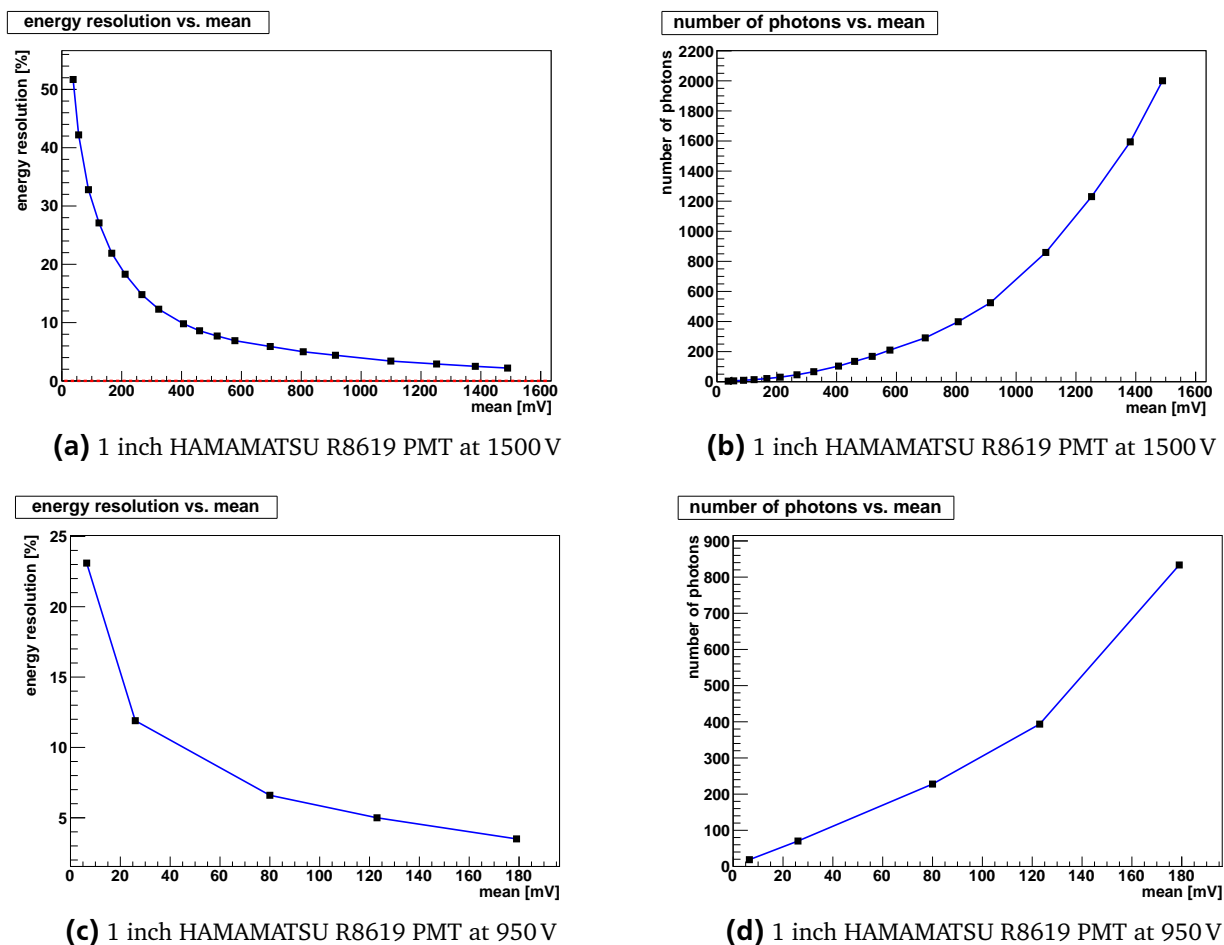


Figure 4.23: Left column: Energy resolution as a function of the PMT output amplitudes, for a module with a 1 inch HAMAMATSU R8619 PMT running at 1500 V and 950 V driven by LED. Right column: The number of detected photons calculated for the different PMT output amplitudes via the first photon statistical approach. By running the PMT at too high supply voltages resulting in saturation of the signal gain, the signal non-linearity is clearly visible.

4.6 Performance tests of HADES ECAL modules with cosmic muons

To understand the response of the HADES ECAL detector to real particles, cosmic muons were used. For them the energy resolution was measured. In this section the main focus will be on the comparison of energy resolution for HADES ECAL modules equipped with the 1 inch HAMAMATSU R8619 and the 3 inch HAMAMATSU R6091 PMTs. Results will be compared to the results from the LED measurement.

4.6.1 Energy resolution comparison of ECAL modules with 1 and 3 inch PMTs

The ECAL module support structure enables the measurement of the detector response with cosmic muons passing through the module as shown in Fig. 4.3. The muon events are triggered by an upper and lower scintillator coincidence measurement. Investigations of cosmic muons were

performed for 1 inch and 3 inch ECAL modules. For this measurement the ECAL modules were located in the support structure, as explained in section 4.1.1. The cosmic muon rate is about 1 event every 180 s. Therefore continuous measurement over several days were performed to get sufficient statistics.

Again an oscilloscope was used as readout electronic and DAQ system. A pulse height measurement of the shaped (20 MHz analogue bandwidth filter and DSP-filter cut-off at 10 MHz) signal was performed with the oscilloscope and the results stored into a histogram. The histogram was analysed with ROOT by fitting a Gaussian plus a linear background to the data. The energy resolution was calculated by a σ/mean ratio obtained from the Gaussian fit. For the 3 inch PMT running at 2000 V an energy resolution of $(8.2 \pm 0.2)\%$ (see Fig. 4.24) was calculated for cosmic muons. For the 1 inch PMT running at 1000 V an energy resolution of $(11.6 \pm 0.2)\%$ (see Fig. 4.25 (right)). Furthermore a pronounced non Gaussian tail towards larger pulse heights is clearly visible for the 1 inch PMT operated in linear range. By running the 1 inch PMT at to high supply voltages, an energy resolution of 8.5% (see Fig. 4.25 (left)) was measured. As shown in section 4.5 non-linearity effects of the gain can shift the resolution to better values. The 1 inch PMT provides a worse energy resolution, in addition the spiky tails (see Fig. 4.15) can cause problems for the readout electronics. Moreover the gain non-linearities at high supply voltages, leading to smaller amplitudes, and therefore limit the dynamical range required for the measurements.

The measured resolution of 8.2% for ECAL modules equipped with the 3 inch HAMAMATSU R6091 PMT for cosmic muons. This is more than a factor 2 larger compared to the one obtained for LED light (see section 4.4.1). This shows that the resolution is dominated by statistical and systematic fluctuations of the Cherenkov light production and absorption process. For example position and direction of the muons traversing the calorimeter module will contribute to deteriorate the resolution.

It is also interesting to compare the measured resolution of 8.2% obtained from cosmic muons, with an expected resolution for electromagnetic showers induced by e^- , e^+ or γ rays with an energy of 1 GeV. For that the measured energy resolution for muons has to be converted. The energy loss for MIPs (Minimum Ionising Particles) in CORNING 25 lead glass (see subsection 2.3 for module properties) can be estimated to be $1.564 \frac{\text{MeV}}{\text{g/cm}^3}$. The total energy loss for MIPs in lead glass with an length of 42 cm is thus $1.564 \frac{\text{MeV}}{\text{g/cm}^3} \cdot 4.06 \frac{\text{g}}{\text{cm}^3} \cdot 42 \text{ cm} = 267 \text{ MeV}$. The average kinetic energy of comic muons is about 2 GeV, the mean kinetic energy is about 4 GeV, at ground. The energy loss increase for 2 GeV muons is about 1.18, thus the total energy loss for cosmic muons is 315 MeV. For this deposited energy an estimated energy resolution of $\frac{4.6\%}{\sqrt{E/\text{GeV}}}$ can be calculated for e^- , e^+ or γ rays with an energy of 1 GeV. By doing the same calculations for cosmic muons with a mean energy of 4 GeV, an estimated energy resolution of $\frac{4.8\%}{\sqrt{E/\text{GeV}}}$ can be calculated for e^- , e^+ or γ . This variation indicates the accuracy of the extrapolation of cosmic muons and electromagnetic showers. It further shows that there is a non negligible contribution of the muon energy loss distribution to the measured resolution for cosmic muon. Unfortunately the energy distribution of the muons in the laboratory is not well known and a quantitative correction difficult.

However, the Cherenkov emission from an electromagnetic shower is more randomised then for muons (see Fig. 2.3). Thus, the $\frac{4.6\%}{\sqrt{E/\text{GeV}}}$ could be considered as a lower limit for the expected

resolution for e^- , e^+ or γ rays with an energy of 1 GeV. The correspondence between Cherenkov light produced and the deposited energy (dominantly ionisation) is not completely independent of the particle species, even if both particles are close to the speed of light limit.

Thus, although the extrapolated values are better than the value of 5% measured by the OPAL collaboration (for a different PMT) [15], by taking into account the error of this estimate the values can be considered comparable.

At the end one can say that only a beam measurement with photons at various energies can clarify above mentioned assumptions and results. A test of ECAL modules with photon beams at the the MAMI-C facility in Mainz is intended for the near future.

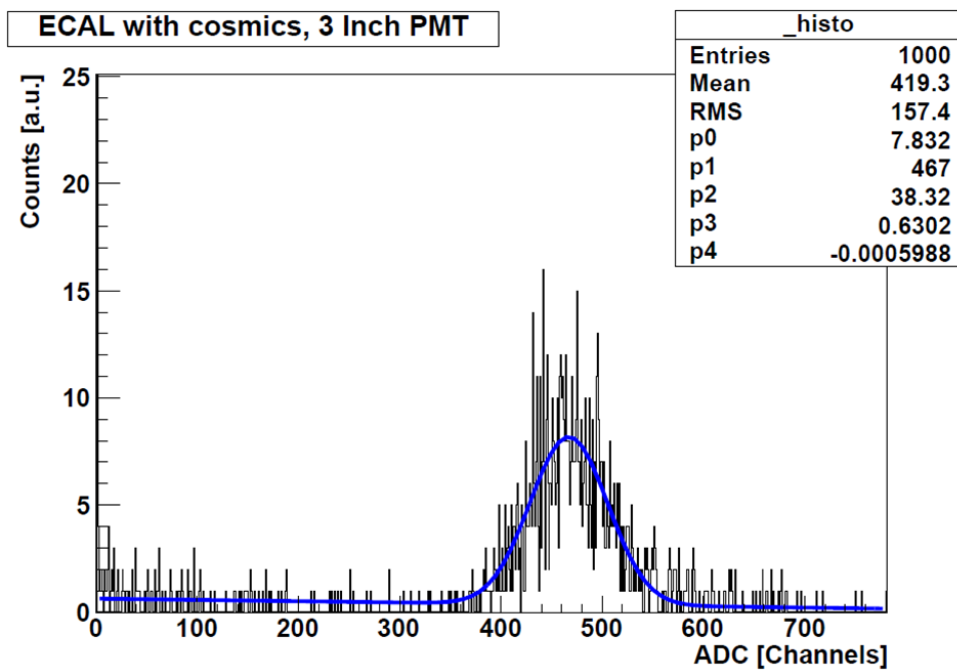
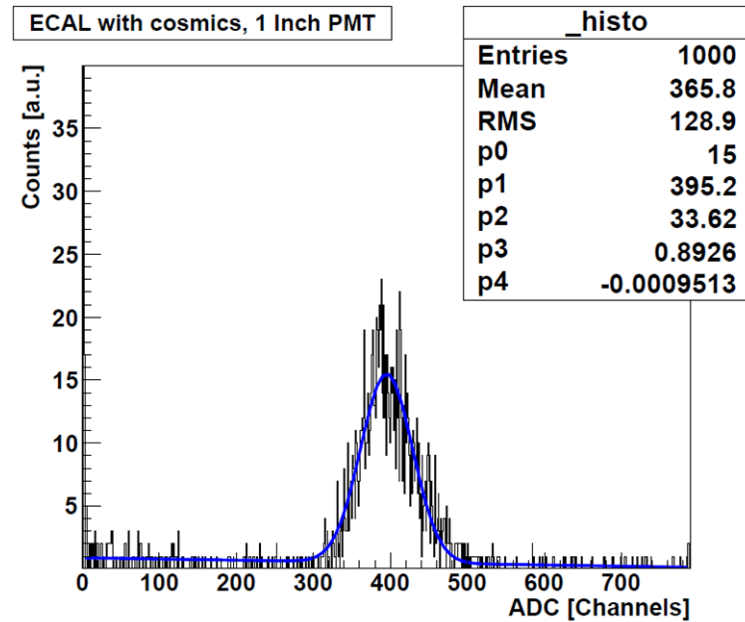
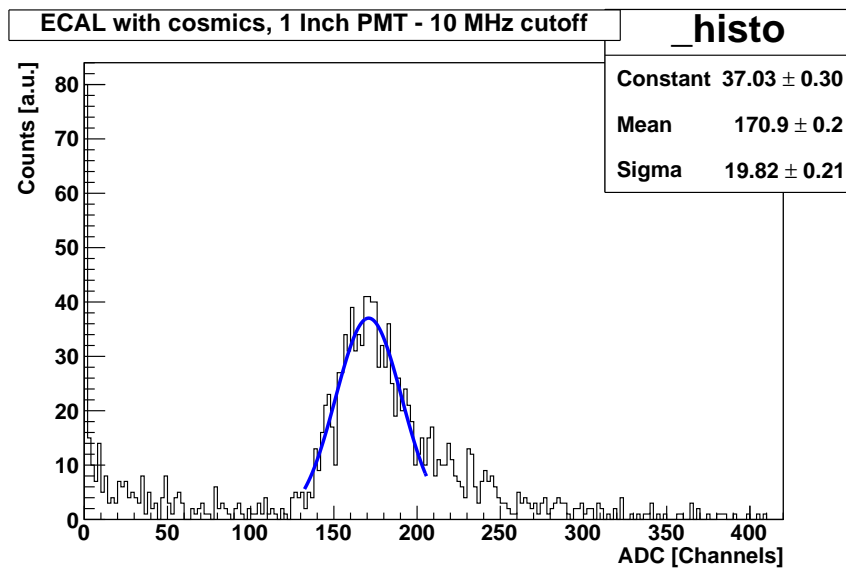


Figure 4.24: Energy resolution of $(8.2 \pm 0.2)\%$ measured for a ECAL module with a 3 inch HAMAMATSU R6091 PMT running at 2000 V for a measurement with cosmic muons. The energy resolution was calculated by the $\sigma(p2)/\text{mean}(p1)$ ratio obtained from a Gaussian fit.



(a) 1 inch PMT at 1500 V



(b) 1 inch PMT at 1000 V

Figure 4.25: Upper panel: An Energy resolution of 8.5% measured for a ECAL module with a 1 inch HAMAMATSU R8619 PMT running at 1500 V for a measurement with cosmic muons. This incorrect value can be archived by running the PMT at too high voltages, where saturation effects of the PMT are dominant. Lower panel: An energy resolution of only $(11.6 \pm 0.2)\%$ can be archived by running the same module with a supply voltage of 1000 V within a linear response range. The energy resolution was calculated by the $\sigma(p2)/\text{mean}(p1)$ ratio obtained from a Gaussian fit.

4.7 First steps towards the PaDiWa AMPS Q2W front-end electronic

For the COME and KISS Q2W readout electronics several tests were performed in order to demonstrate that the FPGA (Lattice MachXO2) implemented on the PaDiWa1 front-end board can be used as a discriminator. A first estimate of the FPGA based discriminator time resolution will be given.

4.7.1 Proof of principle: FPGA used as discriminator

For this measurements a modified PaDiWa1 board, connected to a TRBv3 was used. The components used for these measurements are shown in Fig. 4.26 (left panel). The amplifier of the PaDiWa1 board was removed from two channels, because its limited the signal dynamic range. The first channel was fed with a pulser signal (leading-time: 2.5 ns, width: 89 ns, amplitude: being varied, trailing-time: being varied). A fixed discriminator threshold was set by the TRBv3. The variation of the width of the FPGA LVDS (Low-voltage differential signaling) output was measured by a differential probe of an oscilloscope for different fall-times (decay-slopes).

The input signal and the discriminator output signal are shown in Fig. 4.26 (right panel). In Fig. 4.27 the results of those measurements are shown for three input amplitudes. As expected, the resolution dominantly depends on the decay slope.

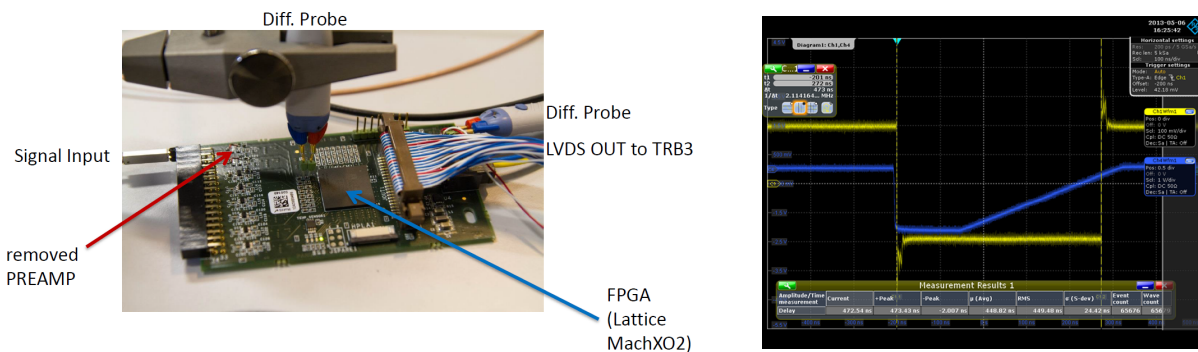


Figure 4.26: Left: For the measurement prepared PaDiWa1 board. Right: The input signal (blue) and discriminator output signal (yellow).

4.7.2 Optimal decay slope for the Q2W electronics

As discussed in section 3.1.2 and shown in Fig. 3.1 for the Q2W charge measurement, the discharge of a capacitor will be forced by a constant current timed by the FPGA resulting in a linear decay. As shown in Fig. 4.27 a shorter fall-time has a particular positive effect on the resolution. This also enables to run the readout electronics at higher frequencies. A lower limit of the decay-time is the time resolution of the TRBv3. A first pulser time measurement with the TRBv3 at the new test set-up provided a time resolution of about 52 ps RMS (see Fig. 4.28). Up to now, with a better FPGA programming, time resolutions of 23 ps can be achieved with the TRBv3 [13].

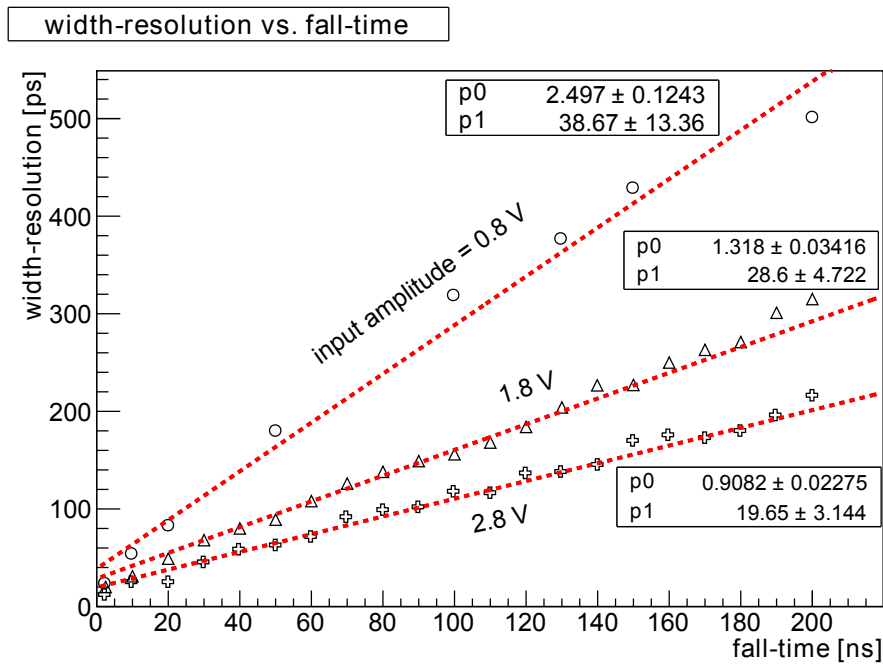


Figure 4.27: Variation of the width (σ) of the FPGA LVDS output was measured by a differential probe of an oscilloscope, for different fall-times. This measurement is shown for three input amplitudes.

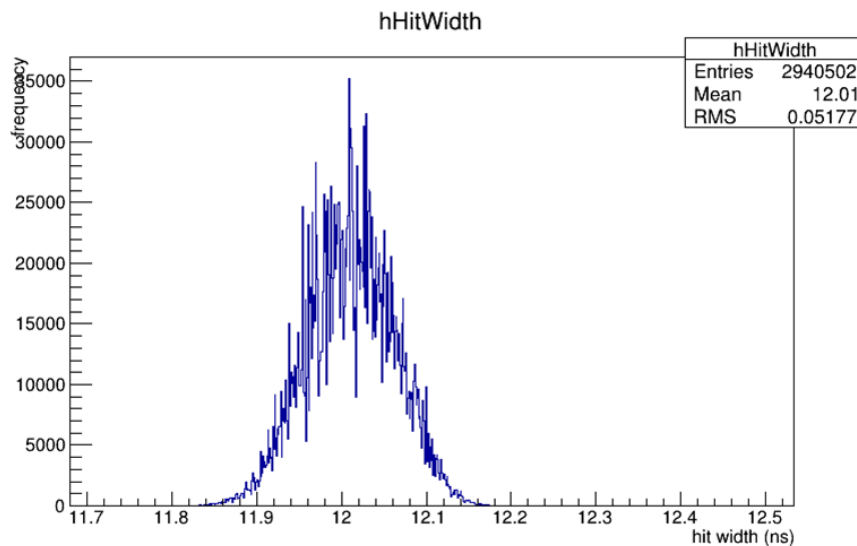


Figure 4.28: Result of a first pulser time measurement with the TRBv3 at the new test set-up. A time resolution of about 52 ps RMS was archived.

4.7.3 Impact of the discriminator resolution onto the relative signal-charge resolution

For a constant slope of 1 V / 50 ns the relative resolution was calculated for different integrator pulse heights. The result is shown in Fig. 4.29. The resolution of the electronics at large pulses is about 0.1%, at small pulses, still a factor 8 better then the expected HADES ECAL resolution ($\frac{5\%}{\sqrt{E[\text{GeV}]}}$). Thus, the front-end electronics based on FPGA's will not deteriorate the ECAL resolution. Adding the estimated electronics resolution to the expected 5% from the calorimeter module quadratically, the deterioration is below 0.1% at 1 GeV

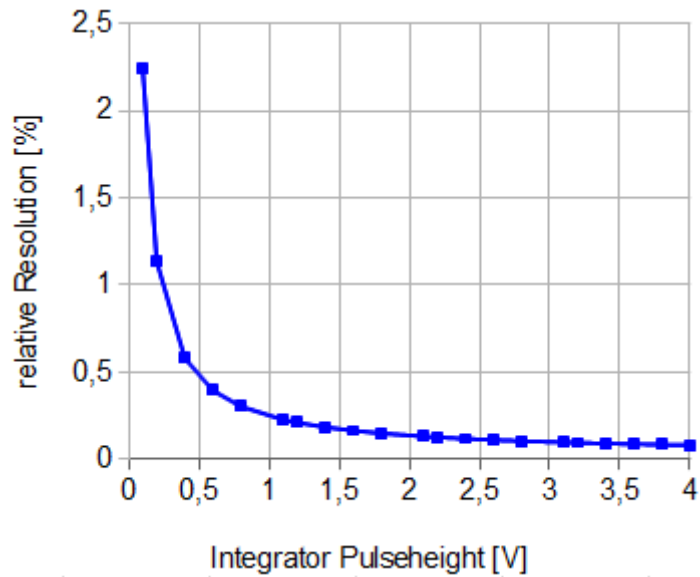


Figure 4.29: Calculated relative charge resolution for signals with a constant decay slope. At integrator pulse heights of about 4 V a resolution of about 0.1% can be achieved.

5 Summary and outlook

The HADES Collaboration aims to explore strongly interacting matter at high baryon densities and moderate temperatures using very rare and penetrating probes. The HADES experiment currently exploits the possibilities of di-electron and strange hadron measurements in elementary as well as heavy-ion collisions up to 2 GeV/u. With the realisation of FAIR, a new possibility will open to study systematically the microscopic properties of strongly interacting matter up to beam energies of 45 GeV/u. The addition of an electromagnetic calorimeter to HADES would allow to measure π^0 , η (essential for extraction of the di-lepton excess), variety of rare strange baryons and will improve electron/pion separation at large momentum ($p > 0.4$ GeV).

An optimisation of the read-out electronics for calorimeters is needed, to achieve individually optimised time and energy measurements including interfacing to the HADES read-out. In the framework of the present work a detailed study of the performance of the future HADES ECAL modules including the read-out electronics is presented.

A method to measure an energy resolution of calorimeters was introduced. Recent developments in designing Time-to-Digital Converters (TDCs) inside standard FPGAs (Field Programmable Gate Arrays) have been proven to be very successfully and enable for a new development of a digitiser and read-out board, the TRBv3. This board is an ideal solution for detectors read-out via Photomultiplier Tubes (PMTs). The TRBv3 will take over the time measurements and data acquisition. The charge measurement of the detector signal will be transformed into a time measurement (charge-to-width: Q2W), by discharge of the integrated signal linear in time.

First tests of the front-end board with the FPGA used as a discriminator. The results show, that the decay slope of the linear discharge should be fast (< 100 ps). The time resolution of the TRBv3 showed an upper limit of 50 ps RMS, however resolution below 23 ps RMS is in reach. It was estimated, that for large integrator pulse heights of about 4 V the electronics resolution is about 0.1%. Test of the full set-up with the so called PaDiWa AMPS front-end board, which is currently manufactured, will be performed in the near future.

To optimise the front-end electronics best to the calorimeters signals, the ECAL modules read-out by PMTs and PSD modules read-out by MAPDs were systematically studied.

Output signals from 1 inch HAMAMATSU R8619 and the 3 inch HAMAMATSU R6091 PMTs were analysed and compared. Spurious pulses were found in the pulse shapes of 3 inch HAMAMATSU R6091 PMTs. Especially prepulses with an amplitude about 10 ns before the mainpulse were observed. These pulses can cause problems for time-of-flight measurements and give an important limitation when setting signal thresholds. It was shown, that characteristic spikes in the tail of the PMT pulses are caused by reflection of Cherenkov light in the module. Also 3 inch HAMAMATSU R6091 PMTs pulse height variations in the pulse amplitude due non-uniformity of light collection and due to magnetic fields were identified. Further investigations on these subjects are on-going.

ECAL modules equipped with 1 inch HAMAMATSU R8619 and 3 inch HAMAMATSU R6091 PMTs were investigated with pulsed LED light. For this an oscilloscope was used as a flexible read-out electronics and DAQ system. With the help of internal signal post processing its intrinsic resolution was improved to less than 0.1%. With this front-end electronic photostatistical effects on the resolution were studied using two approaches, i.e. using the single photoelectron peak and from a statistical approach. From that a lower boundary of the intrinsic energy resolution, caused by photon statistics, was estimated to be about 4%.

By repeating the same measurements with the 1 inch HAMAMATSU R8619 PMT, a gain non-linearity due too high supply voltages was observed, leading to saturation of pulse amplitudes and therefore limiting the dynamic range.

ECAL modules equipped with 3 inch HAMAMATSU R6091 and 1 inch HAMAMATSU R8619 PMTs were further characterised with cosmic muons. The measured energy resolution of 8.2% for ECAL modules equipped with the 3 inch HAMAMATSU R6091 PMT was found. This is more than a factor of 2 larger compared to what was obtained for LED light. This shows that the energy resolution is dominated by statistical and systematic fluctuations of the Cherenkov light production and absorption process.

The measured energy resolution of 8.2% for cosmic muons (average energy of about 2 GeV/c) was converted into an expected energy resolution for electromagnetic showers induced by e^- , e^+ or γ rays with an energy of 1 GeV. An estimated energy resolution of about $\frac{4.8\%}{\sqrt{E/\text{GeV}}}$ was found.

The 1 inch PMT provides a worse energy resolution for cosmic muons of about 11.6%. In addition the spikes observed on the trailing edge of the signal can cause problems for the readout electronics. Moreover the gain non-linearities at high supply voltages, leading to saturation effects in amplitudes, and therefore limit the dynamical range required for the measurements.

It is important to mention, that in beam measurements with photon beams of various energies are needed to verify all the assumptions mentioned above. A test of ECAL modules with photon beams at the MAMI-C facility in Mainz is intended for the near future.

List of Figures

1.1	The HADES experiment	2
1.2	The HADES ECAL detector	3
1.3	The CBM experiment	4
2.1	Interaction of particles with typical a detector arrangement	6
2.2	Idealized electromagnetic shower production in a calorimeter	7
2.3	HGeant2 simulation of the shower production in HADES ECAL modules for different particles	8
2.4	Working principle of a Photomultiplier Tube (PMT)	10
2.5	Illustration of effects leading to PMT spurious pulses	10
2.6	Magnetic characteristics of a PMT, exposed to a magnetic field	11
2.7	Uniformity of light collection of a PMT	12
2.8	The Multi-pixel Avalanche Photo Diode (MAPD)	13
2.9	Schematic view of a HADES ECAL calorimeter module	14
2.10	Schematic view of a CBM PSD prototype module	14
3.1	Sketch of the COME and KISS charge-to-width (Q2W) measurement principle	17
3.2	Intrinsic charge resolution of a Q2W prototype	18
3.3	Layout of the PaDiWa AMPS front-end board	18
3.4	Simulations for the PaDiWa AMPS front-end board	19
4.1	The new test set-up to characterize calorimeter type detectors and their readout electronics	21
4.2	The PMT test-box	22
4.3	Support structure and sketch of a ECAL module set-up for measurements with cosmic muons	23
4.4	The scintillation trigger used to trigger cosmic muons	23
4.5	Sketch of the PSD prototype for the CBM experiment	24
4.6	Typical signal chain of the used oscilloscope (RS 1044)	25
4.7	Oscilloscope display of the raw and shaped pulser signal	25
4.8	The intrinsic resolution (σ/mean) of the used oscilloscope (RS 1044)	26
4.9	Typical amplitude/minimum measurement	26
4.10	Single photo electron peaks of a MAPD	27
4.11	Raw pulse shapes for cosmic muons of ECAL modules	28
4.12	Accumulation of several pulse shapes of a 3 inch HAMAMATSU R6091 PMT	29
4.13	Zoom into a pulse shape of a 3 inch HAMAMATSU R6091 PMT for LED light	30
4.14	Accumulation of pulse shapes of a 3 inch HAMAMATSU R6091 PMT for cosmic muons	30

4.15 Typical pulse shape of a 1 inch Hamamatsu R8619 PMT	31
4.16 Amplitude/gain stability of a 3 inch HAMAMATSU R6091 PMT	32
4.17 Uniformity of light collection of a 3 inch HAMAMATSU R6091 PMT	32
4.18 Illustration of yaw- and roll-rotation of a 3 inch HAMAMATSU R6091 PMT	33
4.19 (Earth) magnetic field influences on 3 inch HAMAMATSU R6091 PMT, without shielding	34
4.20 (Earth) magnetic field influences on 3 inch HAMAMATSU R6091 PMT with shielding	34
4.21 Energy resolution as a function of the PMT output amplitudes for a module with a 3 inch HAMAMATSU R6091 PMT and The number of detected photons calculated for the different PMT output amplitudes via the photo statistical approach	36
4.22 Single photoelectron peak for a ECAL module equipped with a 3 inch HAMAMATSU R6091 PMT	37
4.23 Gain non-linearity of a 1 inch HAMAMATSU R8619 PMT	38
4.24 Energy resolution for a ECAL module with a 3 inch HAMAMATSU R6091 PMT for a measurement with cosmic muons	40
4.25 Energy resolution for a ECAL module with a 1 inch HAMAMATSU R8619 PMT for a measurement with cosmic muons	41
4.26 For the measurement prepared PaDiWa1 board	42
4.27 Variation of the width of the FPGA LVDS output	43
4.28 Result of a first pulser time measurement with the TRBv3	43
4.29 Calculated relative charge resolution for signals with a constant slope	44

Bibliography

- [1] <http://www.lhc-closer.es/1/5/8/0>, September 2013.
- [2] Agakichiev et al. Dielectron production in $^{12}\text{C} + ^{12}\text{C}$ collisions at 2a GeV with the hades spectrometer. *Phys. Rev. Lett.*, 98:052302, Feb 2007.
- [3] et al. Agakichiev. The high-acceptance dielectron spectrometer hades. *The European Physical Journal A*, 41(2):243–277, 2009.
- [4] Agakishiev et al. Inclusive dielectron production in proton-proton collisions at 2.2 gev beam energy. *Phys. Rev. C*, 85:054005, May 2012.
- [5] G. Agakishiev et al. Study of dielectron production in collisions at. *Physics Letters B*, 663(1–2):43 – 48, 2008.
- [6] G Agakishiev et al. Origin of the low-mass electron pair excess in light nucleus-nucleus collisions. *Phys.Lett.*, B690:118–122, 2010.
- [7] S. Aiello et al. The measurement of late-pulses and after-pulses in the large area hamamatsu r7081 photomultiplier with improved quantum-efficiency photocathode. March 2013.
- [8] Prof. Dr. Friedrich H. Balck. Erdmagnetfeld, <http://www2.pe.tu-clausthal.de/agbalck/biosensor/erdmagnetfeld.htm>, September 2013.
- [9] W. Czyzycki, E. Epple, L. Fabbietti, M. Golubeva, F. Guber, et al. Electromagnetic Calorimeter for HADES. 2011.
- [10] B. Friman, C. Höhne, J. Knoll, S. Leupold, J. Randrup, and R. Rapp. *The CBM Physics Book: Compressed Baryonic Matter in Laboratory Experiments*. Lecture Notes in Physics. Springer, 2011.
- [11] I. Frohlich, M. Kajetanowicz, K. Korcyl, W. Krzemien, M. Palka, et al. A General Purpose Trigger and Readout Board for HADES and FAIR-Experiments. *IEEE Trans.Nucl.Sci.*, 55:59–66, 2008.
- [12] J.Prof. Dr. Tetyana Galatyuk. private communication.
- [13] Katrin Große. *GSI Scientific Report 2012 [GSI Report 2013-1]*, volume 2013-1 of *GSI Report*. GSI, Darmstadt, 2013. Wissenschaftlicher Ergebnisbericht der GSI, GSI Annual Report.
- [14] C. Grupen, B. Shwartz, and H. Spieler. *Particle Detectors*. Cambridge Monographs on Particle Physics, Nuclear Physics and Cosmology. Cambridge University Press, 2008.

-
- [15] P.W. Jeffreys, M. Akrawy, G.T.J. Arnison, J.R. Batley, Kenneth Watson Bell, et al. Development Studies for the Opal Endcap Electromagnetic Calorimeter Using Vacuum Photo Triode Instrumented Lead Glass. *Nucl.Instrum.Meth.*, A290:76, 1990.
- [16] Behruz Kardan. private communication.
- [17] Hamamatsu Photonics K.K. *PHOTOMULTIPLIER TUBES - Basics and Applications (THIRD EDITION (Edition 3a))*. HAMAMATSU PHOTONICS K. K., 2007.
- [18] Hamamatsu Photonics K.K. *OPTO-SEMICONDUCTOR HANDBOOK (First edition)*. HAMAMATSU PHOTONICS K. K., 2010.
- [19] Dr. Ilse Koenig. private communication.
- [20] Dr. Wolfgang Koenig. private communication.
- [21] J. Michel et al. The upgraded HADES trigger and data acquisition system. *JINST*, 6:C12056, 2011.
- [22] Photonis. *Photomultiplier tubes: Principle & Applications*. Photonis, 2002.
- [23] Dušan Ponikvar. Wilkinson-type {ADC} with short conversion time and low clock frequency. *Nuclear Instruments and Methods in Physics Research Section A: Accelerators, Spectrometers, Detectors and Associated Equipment*, 408(2–3):523 – 529, 1998.
- [24] S.Ogio et al. Proceedings of the 31th icrc in łódz (2009) id811.
- [25] The {OPAL} detector at {LEP}. *Nuclear Instruments and Methods in Physics Research Section A: Accelerators, Spectrometers, Detectors and Associated Equipment*, 305(2):275 – 319, 1991.
- [26] Dr. Pavel Tlustý. private communication.
- [27] Dr. Michael Traxler. private communication.
- [28] C Ugur, E Bayer, N Kurz, and M Traxler. A 16 channel high resolution (<11 ps rms) time-to-digital converter in a field programmable gate array. *Journal of Instrumentation*, 7(02):C02004, 2012.
- [29] C Ugur, W Koenig, J Michel, M Palka, and M Traxler. Field programmable gate array based data digitisation with commercial elements. *Journal of Instrumentation*, 8(01):C01035, 2013.
- [30] The PSD Workgroup and the CBM Collaboration. Technical design report for the cbm projectile spectator detector (psd). March 2013.

Danksagungen

An dieser Stelle möchte ich mich bei allen Personen herzlichst bedanken, die mich bei der Erstellung dieser Arbeit unterstützt haben:

Ein großer Dank geht an meine Betreuerin J.Prof. Dr. Tetyana Galatyuk, welche mich herzlichst in ihre Arbeitsgruppe aufgenommen hat. Besonders stolz bin ich, dass ich mithelfen durfte ihr neues Labor aufzubauen um dort viel neues entdecken und selber ausprobieren zu können.

Ein weiterer großer Dank geht an meinen Betreuer Dr. Wolfgang Koenig, durch seine herzhaften Erklärungen konnte ich sehr viel mitnehmen. Er hat mich immer wieder mit interessanten neuen Anregungen und Ideen versorgt.

Ich danke der Nachwuchsgruppe VIP-QM: Georgy Kornakov, Malgorzata Gumberidze und Szymon Harabasz für die netten Stunden in unsere Arbeitsgruppe.

Ich danke Eugen Bayer, Michael Traxler und Behruz Kardan für die lehrreichen und interessanten Labor-Sitzungen.

Ich danke Pavel Tlusty, Ondrej Svoboda und Yuri Sobolev für die sehr intensiven und sehr lehrreichen ECAL Messwochen an der GSI.

Ich danke Jochen Markert und Georgy Kornakov für die Anregungen und Korrekturen und Ilse Koenig für die Simulationen.

Ich danke der HADES-ECAL Gruppe.

Ich danke der HADES-ALL, HADES-GSI und HADES-Young-Members Gruppe für die herzliche Aufnahme in die Kollaboration.

Ich danke meinen Eltern, Großeltern und Freunde welche immer für mich da sind.